minerals

MDPI

Article

Late Permian High-Ti and Low-Ti Basalts in the Songpan–Ganzi Terrane: Continental Breakup of the Western Margin of the South China Block

Yumeng Shao [1], Danping Yan [1,*], Liang Qiu [1], Hongxu Mu [1,2] and Yi Zhang [1]

[1] School of Earth Sciences and Resources, China University of Geosciences, Beijing 100083, China
[2] Beijing Research Institute of Uranium Geology, Beijing 100029, China
* Correspondence: yandp@cugb.edu.cn

Abstract: Although the Emeishan Large Igneous Province (ELIP) has been thoroughly researched, the role of the ELIP in the tectonics of the Songpan–Ganzi extensional basin in the eastern Tibetan Plateau has long been argued without any corroborated and robust evidence. We have investigated the basalt succession of the Dashibao Formation along Xindianzi and Xuecheng sections in the southeast margin of the Songpan–Ganzi Terrane (SGT). New SIMS zircon U-Pb ages and geochemical features of the Dashibao Formation are reported in this paper. Zircons of basalt sample XDZ02-1 yielded a weighted mean age of 259.1 ± 1.66 Ma, which is in alignment with the period when the main eruption of the ELIP occurred. Zircons from two tuff samples XDZ05-1 and XC05-2, overlying the basalt succession, were dated at 251.8 ± 1.57 Ma and 251.5 ± 0.27 Ma, respectively. These new dating results revealed a ~10 Ma eruption for the Dashibao basalts. The Dashibao basalts are geochemically classified into alkaline basalts (Group 1) and tholeiitic basalts (Group 2), which are a part of the Emeishan basalt. We thus propose that the Dashibao basalts erupted in a continental rift setting, located at the margin of the ELIP. The temporal and spatial coincidence of the Dashibao basalt, ELIP, and continental rifting in the western margin of the South China Block suggest that the continental breakup is a response to the Permian mantle plume that triggered the separation of the SGT in the eastern Tibetan Plateau.

Keywords: Dashibao basalts (Dashibao Formation); continental rift; Emeishan Large Igneous Province (ELIP); Songpan–Ganzi Terrane (SGT)

check for updates

Citation: Shao, Y.; Yan, D.; Qiu, L.; Mu, H.; Zhang, Y. Late Permian High-Ti and Low-Ti Basalts in the Songpan–Ganzi Terrane: Continental Breakup of the Western Margin of the South China Block. *Minerals* **2022**, *12*, 1391. https://doi.org/10.3390/min12111391

Academic Editor: Alexey V. Ivanov

Received: 14 September 2022
Accepted: 28 October 2022
Published: 31 October 2022

Publisher's Note: MDPI stays neutral with regard to jurisdictional claims in published maps and institutional affiliations.

Copyright: © 2022 by the authors. Licensee MDPI, Basel, Switzerland. This article is an open access article distributed under the terms and conditions of the Creative Commons Attribution (CC BY) license (https://creativecommons.org/licenses/by/4.0/).

1. Introduction

Research indicates that flood basalt and continental rift regularly interact [1–12]. The Emeishan Large Igneous Province (ELIP), largely distributed along southwestern China and the eastern Qinghai–Tibet Plateau, has been extensively studied [13,14]. Due to the geochemical and petrological composition, paleontological correlation, geophysical structure, and geochronological constraints, a mantle plume origin has been suggested [15–24]. However, the role of the ELIP in the tectonics of the South China Block and the eastern Tibetan Plateau is not yet understood. In particular, the correlation between the ELIP and the Songpan–Ganzi extensional basin in the eastern Tibetan Plateau has long been argued without any corroborated and robust evidence [16,25–28].

The Dashibao Formation, also named the Dashibao basalts, was separated from the main body of the ELIP by the breakup of the western margin of the South China Block during the Permian–Triassic period and exposed along the south of the NE-striking Longmen Shan tectonic belt [13,14]. Its petrogenesis and precise geochronology can provide some key constraints on the nature of the mantle source and the genetic relationship between the ELIP and the rift of the SGT. Although the Dashibao basalts have been closely related to the ELIP in publications, nature and tectonic implication, especially its exact eruption age, have been rarely documented [26,28,29].

In this study, we present new SIMS U-Pb zircon ages, whole rock major and trace elements geochemistry, and Sr-Nd isotopes of the Dashibao basalt in the Xindianzi area. These new data in conjunction with prior data: (1) address the petrogenesis of of Dashibao basalts; (2) constrain the duration of the Dashibao basalt eruption; and (3) highlight the significance of the Emeishan mantle plume in the regional tectonic development and origin of the SGT.

2. Geological Background

2.1. Songpan–Ganzi Terrane

The SGT is massive and triangle-shaped, with an area of more than 200,000 km^2 [30] (Figure 1). The SGT is separated from South China Block to the east by the Longmen Shan tectonic belt and from the Qinling–Dabie orogenic belt by Kunlun–Animaqing suture to the north. To the southwest, the SGT is separated from the Qiangtang Terrane by Jinsha suture [31] (Figure 1). Previous research speculated a basement of the South China Block beneath the SGT based on stratigraphic correlation, as well as geochemical characteristics and high-precision reflection profile across the SGT and South China Block. Such a close correlation implies that the SGT was connected with South China Block at least until the late Permian [32–35] (Figure 1b). Only a few Pre-Triassic strata and Neoproterozoic basements are exposed along the eastern and southern margins of SGT; the remainder is almost entirely filled with 5–10 km of folded Triassic flysch that sharply contrasts with the pre-Permian platform setting [13,14,36,37]. It has been interpreted as a remnant ocean basin [37,38] or a Permian–Triassic rift basin that developed at a triple junction [16,25,28,39].

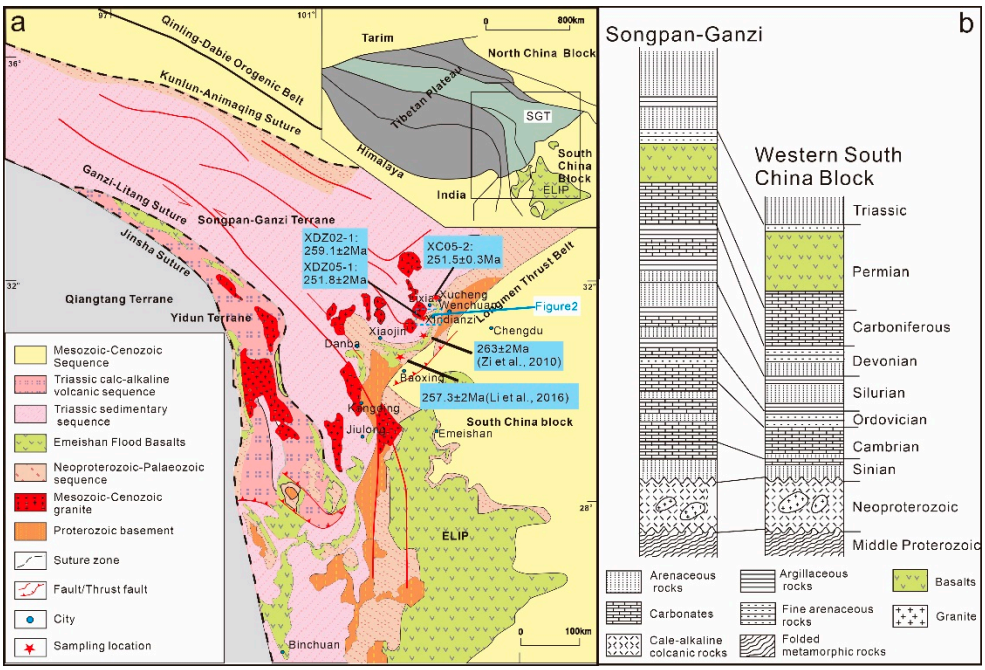


Figure 1. (**a**) Regional geological sketch of the Songpan–Ganzi Terrane (SGT), South China Block and their adjacent areas [26]. (**b**) Stratigraphic correlation of the Proterozoic metamorphic basement, the Paleozoic to Triassic sedimentary sequences in the SGT and western margin of the South China Block [13,14,26].

2.2. The Emeishan Large Igneous Province (ELIP)

The ELIP basalt is distributed in the southwestern South China Block and the eastern part of the Tibetan Plateau [40]. Recent studies have also distinguished Late Permian flood basalts outside of the previously defined ELIP, such as high-Ti basalt in the western part of Guangxi Province in Southwest China [41], marine-altered basalt in the southern SGT [16,26,28,29], and massive, or pillowed high-Ti basaltic lava in the northeastern Sichuan

basin [13,14,16]. These new findings indicate that the initial coverage of ELIP has reached 7×10^5 km^2 [42].

The ELIP basalt sequence lies between the Middle Permian limestone of the Maokou Formation and the Late Permian sandstone and mudstone of the Xuanwei Formation. The thickness of lava mounds ranges from several hundred meters to five kilometers [20,40]. The sequence consists primarily of flood basalt and pyroclastic rocks, with minor amounts of picrite, basaltic andesite and alkaline felsic rocks [20,26,42–44] believed to have originated from a mantle plume in the Late Permian [20,45].

2.3. Dashibao Formation Basalts

The Dashibao Formation basalt (Dashibao basalts) lies along the boundary between South China Block and SGT (Figure 1a) [13,14,16,28,29]. The basalt exposed in areas of Lixian, Wenchuan, Baoxing, Xiaojin, Danba, Kangding and Jiulong extends over 400 km along the NE-striking southern Longmen Shan tectonic belt [13,14,26,29] (Figure 1a). The basalt gradually decreases in thickness from southwest to northeast and finally vanishes in the Xucheng area [13,14].

The Dashibao basalt is unconformably sandwiched between the underlying brecciated bioclastic limestone of the Sandaoqiao Fm. and the overlying marl, tuffaceous siltstone and sericite phyllite tuffaceous siltstone and sericite phyllite of Bocigou Fm. The Dashibao basalt includes multiple flows with pillow lava, with flow top pyroclastics and thin sedimentary intercalations, which indicate multiple submarine eruptions [13,14,26].

3. Materials and Methods

3.1. Petrography of the Dashibao Basalt in the Xindianzi Area

Two representative geological sections, 1 and 2, were investigated in detail with rock type, assemblage, and geological relation Figure 2b). Exposed Dashibao basalts sequence in the Xindianzi area is 50 m thick. All basalt rocks have massive (local pillow) structures that were altered (Figure 3a,b). The basalt has porphyritic texture with plagioclase phenocrysts (5~10%) altered into sericite. The intergranular groundmass consists of fine-grain plagioclase, pyroxene, Fe-Ti oxides and biotite. Clinopyroxene is extensively altered to chlorite (Figure 3c–f).

3.2. Analytical Methods

U-Pb zircon dating was performed at the Beijing Research Institute of Uranium Geology using the CAMECA IMS-1280HR ion microprobe. We use the shape and mono collector modes to determine zircon U-Pb ages [46]. Whole-rock major element oxides were analyzed using a Leeman Prodigy inductively coupled plasma–optical emission spectrometer (ICP-OES), and trace element analyses for basalt samples were conducted using an Agilent-7500a quadrupole inductively coupled plasma–mass spectrometer (ICP-MS) at the Elemental Geochemistry Lab in the Institute of Earth Sciences, China University of Geosciences, Beijing (CUGB) [47]. Sr–Nd isotope measurements were performed by a multi-multi-collector-inductively coupled plasma-mass spectrometer (MC-ICP-MS) at the Isotope Geochemistry Laboratory of the China University of Geosciences, Beijing (CUGB). Detailed analyses are shown in the Supplementary Materials [48–50].

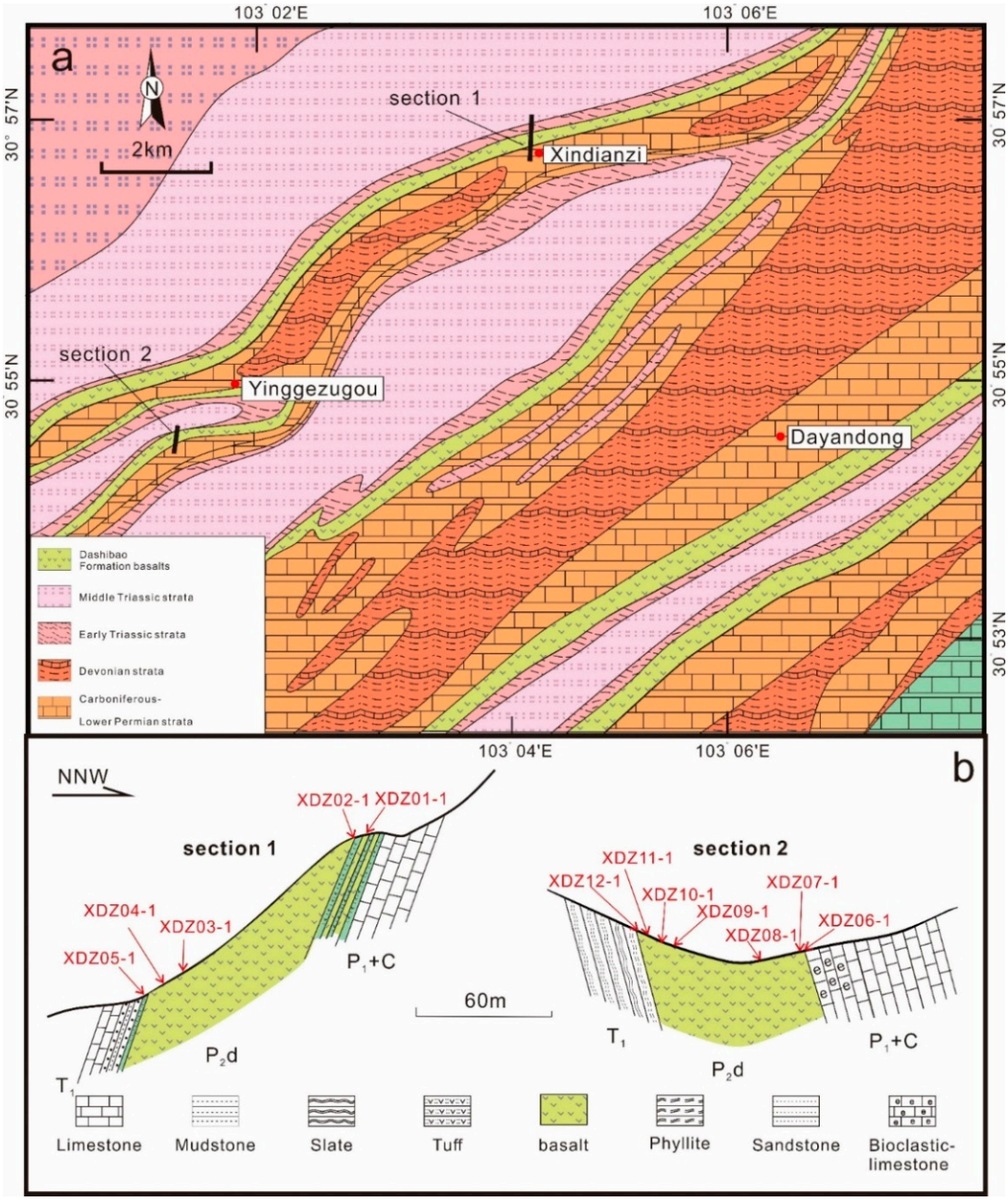


Figure 2. (**a**) Schematic geological map of the Xindianzi area (modified after [13,14]). (**b**) Geological Sections 1 and 2 with Dashibao basalt and sample location.

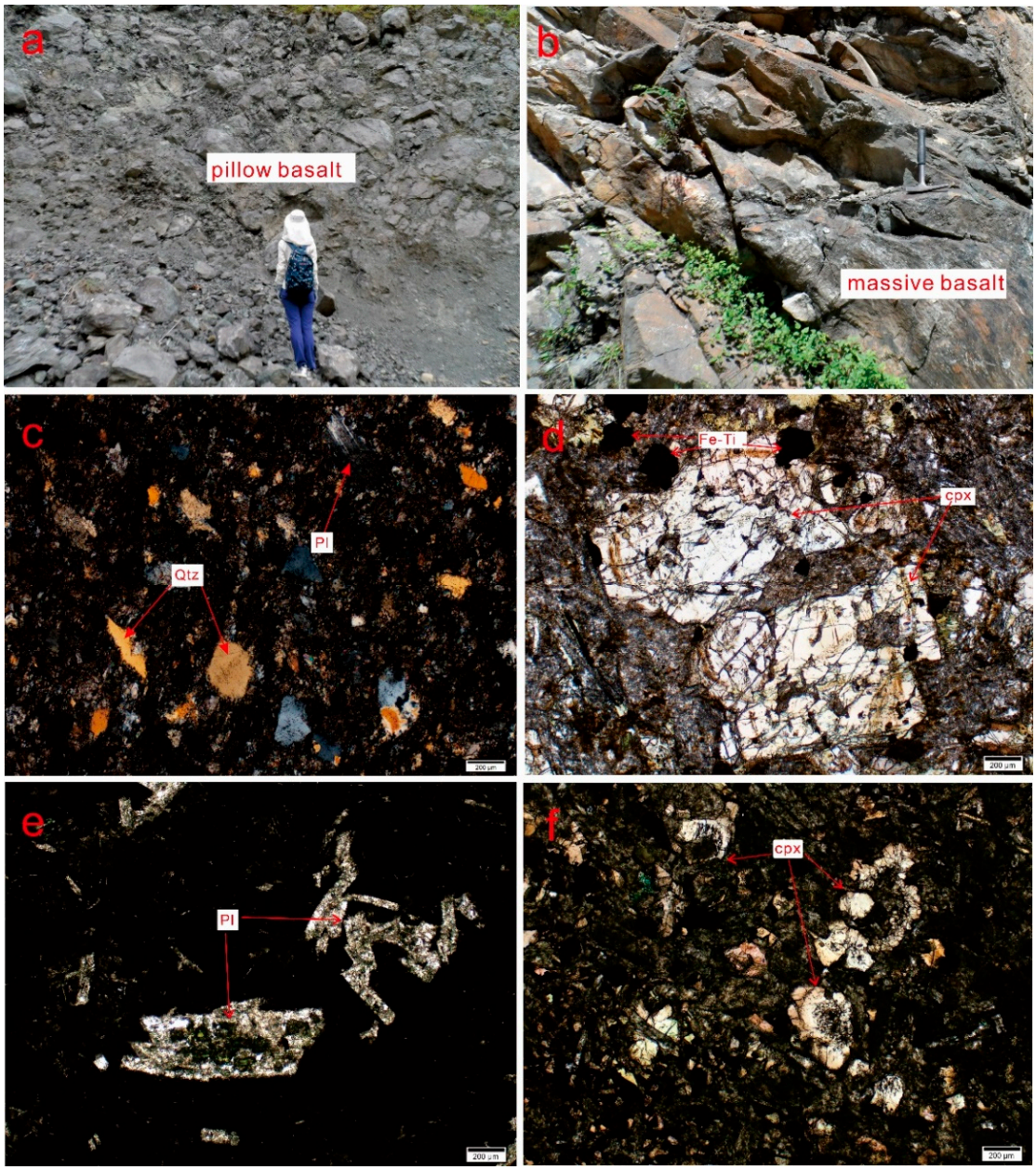


Figure 3. Field and representative photomicrographs of the Dashibao basalt in the Xindianzi area. (**a**) Pillow lavas; (**b**) massive basalt; (**c**) tuff sample containing quartz, feldspar crystal; (**d**) Fe-Ti oxides and clinopyroxene phenocrysts in Group1 basalts; (**e**) plagioclase phenocrysts in Group2 basalt; (**f**) clinopyroxene phenocrysts in Group1 basalt. Pl. plagioclase; Cpx. clinopyroxene; Qtz. quartz; Fe-Ti. Fe-Ti oxides.

4. Results

4.1. SIMS Zircon U-Pb Age

To determine the eruption time of volcanic rocks, several alternative volcanic tuff samples and basalt samples were collected from Sections 1 and 2 (Figures 2 and 3). Three samples, basalt sample XDZ02-1 and tuff samples XDZ05-1 and XC05-2, were selected for zircon separation and zircon U-Pb dating. SIMS zircon U–Pb analyses for samples XDZ02-1, XDZ05-1 and XC05-2 are listed in Supplementary Table S1 and illustrated in Concordia plots and cathodoluminescence (CL) images (Figure 4). The analytical results will be described separately.

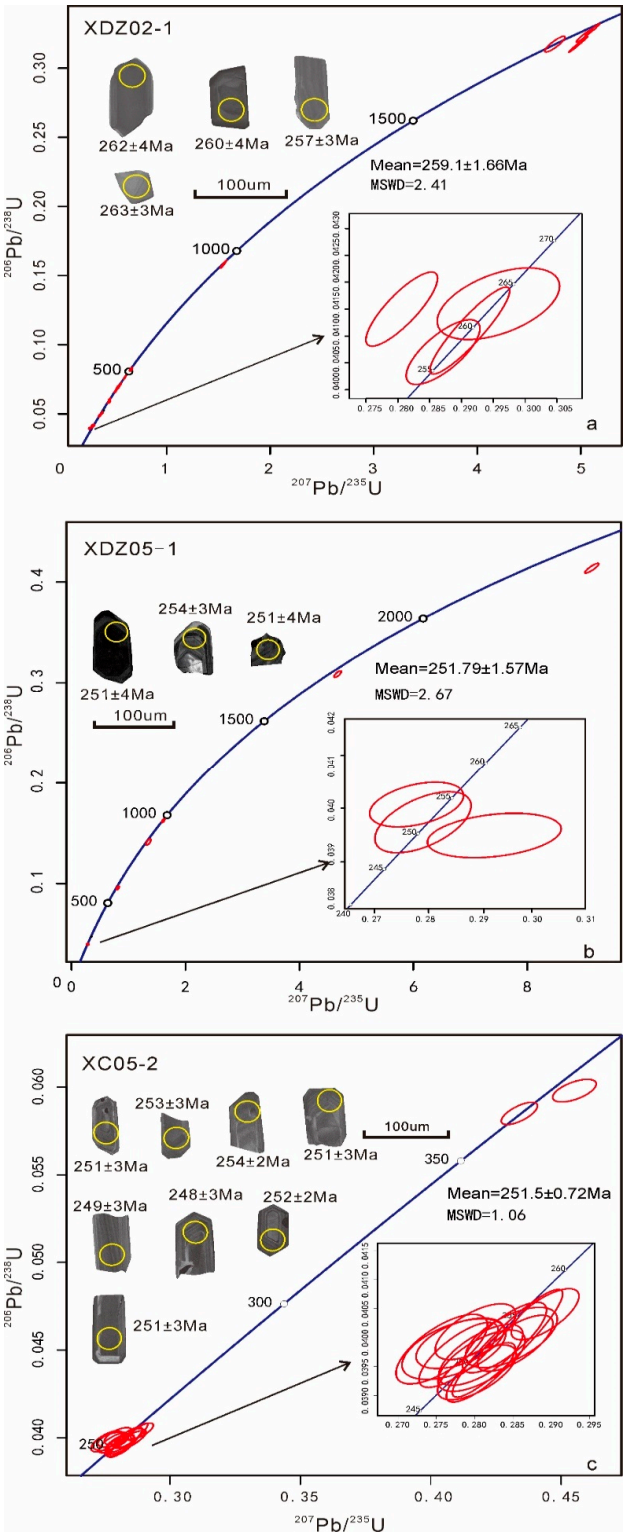


Figure 4. (**a**–**c**) SIMS zircon U-Pb concordia diagram, and corresponding CL images of repre sentative zircons for basalt sample XDZ02-1 and tuff samples XDZ05-1 and XC05-2 (circles refer to analyzed spots).

Basalt sample XDZ02-1 was collected in Section 1. Zircons from XDZ02-1 mostly have a long prismatic shape with oscillatory zonation in CL images, lengths ranging from 50 to 110 µm, and ratios of length to width ranging from 1:1 to 4:1 (Figures 2 and 4b). These zircons are generally high in Th and U concentrations with Th/U ratios varying from 0.28 to 0.91 and an average of 0.60, reflecting magmatic origin [51–55]. Four zircon grains yielded

a weighted mean $^{206}Pb/^{238}U$ age of 259.1 ± 1.66 Ma (N = 4, MSWD = 2.41) (Supplementary Table S1), which represents the age of basalt crystallization, while 18 excluded zircon grains have significantly older ages of 316 Ma to 1805 Ma and are presumably inherited (Figure 4, Supplementary Table S1).

Tuff sample XDZ05-1 was collected from the top part of the Dashibao basalts in Section 1. Zircons from XDZ05-1 mostly have a long prismatic shape with oscillatory zonation in CL images, lengths ranging from 50 to 150 μm, and ratios of length to width ranging from 1:1 to 3:1 (Figures 2 and 4a). These zircons are generally high in Th and U concentrations with Th/U ratios varying from 0.1 to 1.3 and an average of 0.72, reflecting magmatic origin [51–55]. Three zircon grains yielded a weighted mean $^{206}Pb/^{238}U$ age of 251 ± 1.57 Ma (N = 3, MSWD = 2.67) (Supplementary Table S1), which represents the age of basalt crystallization, while six excluded grains have significantly older ages of 589 Ma~2232 Ma and are presumably inherited zircons.

Tuff sample XC05-2 was collected from the top of the Dashibao basalts in the Xuecheng section. Zircons from XC05-2 mostly have a long prismatic shape with oscillatory zonation in cathodoluminescence images, lengths ranging from 50 to 150, and length-to-width ratios ranging from 1:1 to 3:1 (Figures 1 and 4c). These zircons generally have high Th and U concentrations with Th/U ratios varying from 0.16 to 0.91 and an average of 0.50, reflecting magmatic origin [51–55]. A total of 14 zircon grains yielded a weighted mean $^{206}Pb/^{238}U$ age of 251.5 ± 0.27 Ma (N = 14, MSWD = 1.06) (Supplementary Table S1), which represents the age of basalt crystallization, while two excluded grains have significantly older ages of 367 Ma and 375 Ma, and are presumably inherited.

4.2. Whole-Rock Geochemistry

Samples for elemental composition from the Dashibao basalts in the Xindianzi area are listed in Supplementary Table S2. As noted above, the samples display alteration features (Supplementary Table S2, Figure 3), reflected by high loss on ignition (LOI) ranging from 2.54 to 4.84. For comparison all major element contents were normalized to 100% on a volatile-free basis prior to plotting.

Basalts along Sections 1 and 2 have essential different geochemical properties. Two rock types, Group 1 and Group 2, were chemically divided based on the content of TiO_2, Ti/Y ratio, Th/Nb ratio and Mg# [20,21,44].

Group 1 displays SiO_2 = 48.00 to 53.10 wt%, TiO_2 = 3.02 to 4.29 wt%, Al_2O_3 = 14.27 to 16.33 wt%, MgO = 3.76 to 5.06 wt% (Mg# = 36 to 41), CaO = 5.66 to 8.94 wt%, TFe_2O_3 = 13.01 to 14.6 wt%, and P_2O_5 = 0.32 to 0.45 wt%. The $Na_2O + K_2O$ = 3.66 to 4.95 wt%. Group 1 is characterized by high-Ti (HTi) with $Ti0_2$ > 2.5% and Ti/Y > 500 (Figure 5) [20,21,44]. In the Nb/Y vs. Zr/TiO_2 diagram, Group 1 is plotted in the alkaline basalt field (Figure 6a) [56,57].

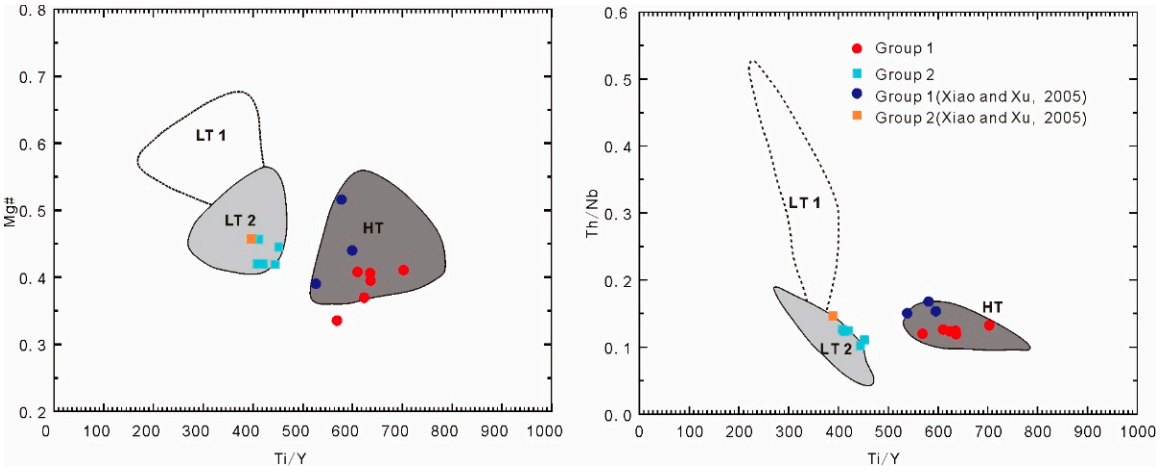


Figure 5. Diagrams showing the variation of Mg# and Th/Nb against Ti/Y for the Emeishan basalts. Shaded areas indicate the domains of the Emeishan basalts from the Binchuan area [20,44].

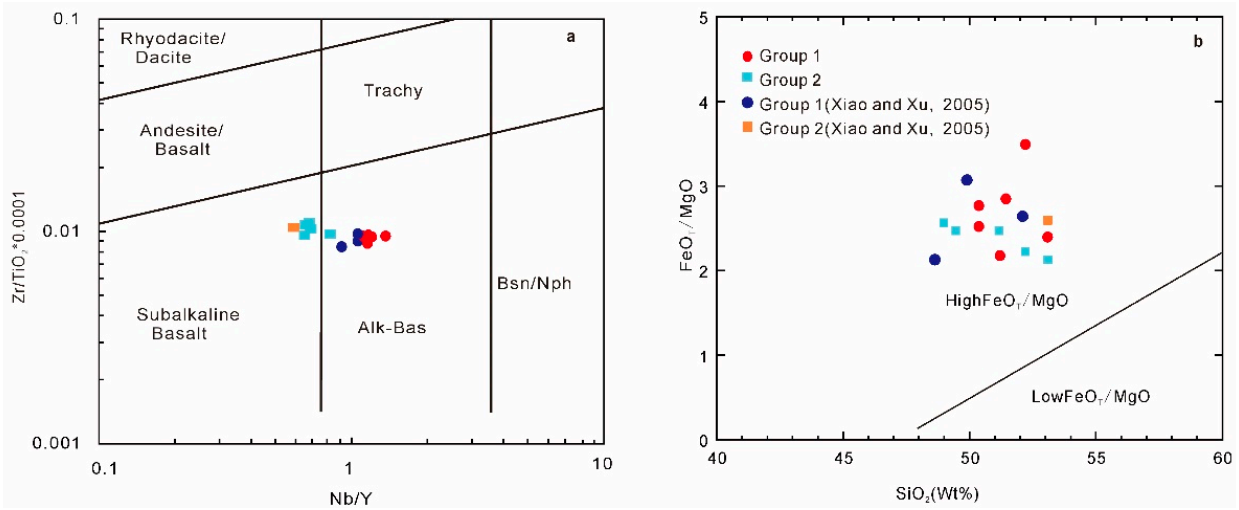


Figure 6. (**a**) Nb/Y vs. Zr/TiO_2 diagram [56]; (**b**) SiO_2 vs. FeO_T/MgO diagram [57].

Group 2 basalts display SiO_2 = 49.46 to 53.10 wt%, and TiO_2 = 2.27 to 2.58 wt%. The TiO_2 content is slightly lower than the typical OIB basalt (TiO_2 = 2.87% [58], Al_2O_3 = 13.62 to 14.47 wt%, MgO = 5.10 to 5.54 wt% (Mg# = 42–46), CaO = 7.07 to 8.80 wt%, TFe_2O_3 = 13.09 to 14.51 wt%, and P_2O_5 = 0.29 to 0.35 wt%. The $Na_2O + K_2O$ = 3.85 to 4.83 wt%. Group 2 is characterized by low-Ti (LTi) with $Ti0_2$ < 2.5% and Ti/Y < 500 (Figure 5) [20,44]. In the Nb/Y vs. Zr/TiO_2 diagram, Group 2 is plotted in the subalkaline series field, and in the SiO_2 vs. FeO_t/MgO diagram, almost all LTi samples show a tholeiitic trend (Figure 6) [56,57].

In summary, Group 1 basalts have relatively high TiO_2, Al_2O_3, and P_2O_5 with lower MgO and CaO. The Group 1 basalts with Mg# = 36 to 41 are more evolved than the Group 2 with Mg# = 42–46) [59].

Trace element contents and patterns of the Dashibao basalt in the Xindianzi area are shown in Supplementary Table S2 and Figure 7. Group 1 is alkaline basalt that displays Total Rare Earth Element (∑REE) = 209–280 ppm, $(La/Yb)_N$ = 10.5–12.0, $(La/Sm)_N$ = 2.4–2.6, (Gd/Yb) = 3.0–3.2, and has high LILE (large ion lithophile elements), HSFE (high strength field elements) and REE (rare earth elements) contents (Supplementary Table S2). This group is characterized by highly fractionated LREE/HREE chondrite-normalized patterns with no significant Eu anomaly (δEu = 0.8–1.0). The primitive-mantle normalized trace elements spider diagram exhibits patterns very similar to OIB and akin to those of the HTi basalts the ELIP [20,44] (Figure 7).

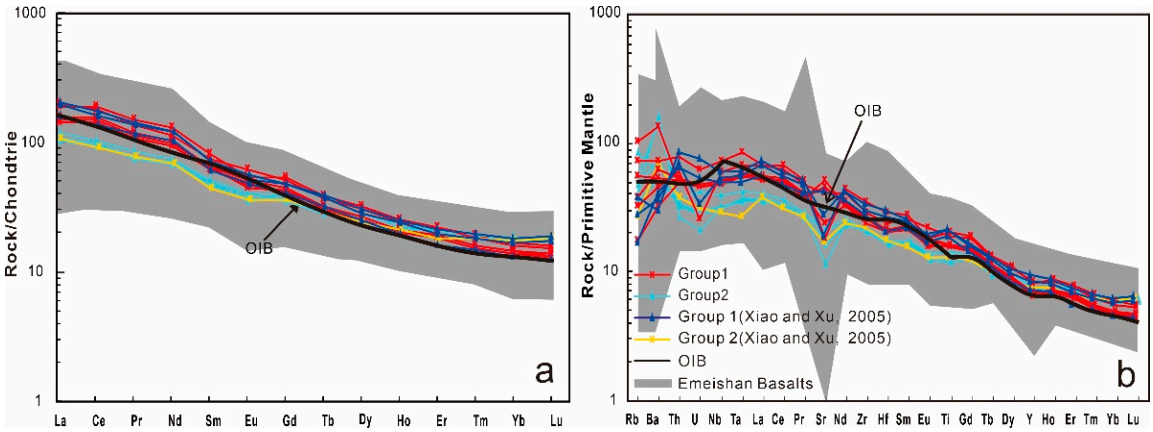


Figure 7. (**a**) Chondrite-normalized REE pattern distributions and (**b**) primitive-mantle-normalized trace element spider diagrams for Dashibao basalts in the Xindianzi area. Normalizing values for chondrite and primitive mantle are from [58], and the average composition of OIB is after [58]. Shaded areas are plotted Emeishan basalts [60].

Group 2 corresponds to tholeiitic basalt that displays ∑REE = 154–168 ppm, $(La/Yb)_N$ = 5.9–6.5, $(La/Sm)_N$ = 2.2–2.3, and $(Gd/Yb)_N$ = 2.1–2.2 (Supplementary Table S2). This group is characterized by highly fractionated LREE/HREE chondrite-normalized patterns, LREE enrichment, and negligible Eu negative anomalies (δEu = 0.8–1.00) in the primitive-mantle-normalized trace elements spider-diagram (Figure 4). Group 2 displays Th, U, Nb, Ta, La, Ce, and Sr negative anomalies. The composition of Group 2 is similar to the low-Ti basalt in ELIP [20,44].

Overall, REE and trace element patterns of the Dashibao basalt in the Xindianzi area are similar to the OIB type [58] and are close to the average Emeishan basalt field [58] (Figure 7).

4.3. Sr-Nd Isotope Ratios

The whole-rock Sr-Nd isotopic compositions of four alkaline basalts in Group1 and six subalkaline basalts in Group 2 of Dashibao basalts in the Xindianzi area are presented in Supplementary Table S3 and Figure 8. The initial isotopic values were corrected to 260 Ma. Group 1 basalts have a small range of age-corrected $^{87}Sr/^{86}Sr$ = 0.705790–0.706488, $^{143}Nd/^{144}Nd$ = 0.5123486–0.5125122, εNd(t) = 0.9–4.0, and Group 2 basalts display $^{87}Sr/^{86}Sr$ = 0.7039757–0.706999, $^{143}Nd/^{144}Nd$ = 0.5123068–0.5123879, and εNd(t) = 0.04–1.6. In Figure 8, most of the Group 1 and Group 2 basalts are similar to those of modern plume-related OIB [35,40] and Emeishan basalts [16,60].

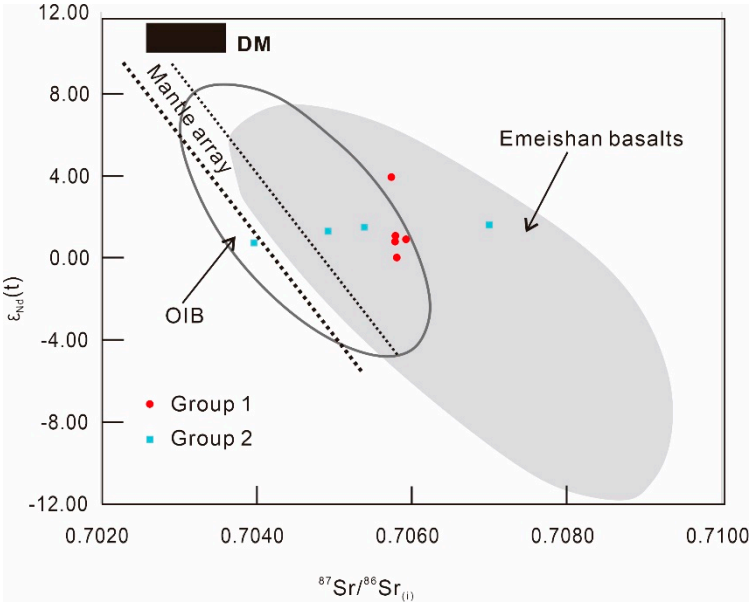


Figure 8. Sr−Nd isotopic compositions of the Dashibao basalts in the Xindianzi area. Emeishan basalts are according to [61], and DM (depleted mantle) is according to [58].

5. Discussion

5.1. Petrogenesis

5.1.1. Fractional Crystallization

Low Mg# = 34–46 ppm, Cr = 41–121 ppm, and Ni = 49–77 ppm levels in the Dashibao basalts are noticeably lower than Mg# = 73–81, Cr > 1000 ppm, and Ni > 400 ppm levels in primitive unfractionated mantle magmas [62], indicating fractional crystallization for the magmas. Since Cr, Ni, and Co are mainly present in olivine, pyroxene, and other minerals, the contents of these elements often reflect the separation and crystallization of olivine minerals in magma [63]. The low compatible elements in Group 1 (Cr = 41–63, Ni = 49–75, Co = 39–48) show fractionation of olivine and clinopyroxene. The correlation between Ni, V, and Cr suggests that different degrees of clinopyroxene-and olivine-controlled fractionation may have occurred in the primary magma of the Dashibao basalts. Most

Group 1 basalts show no Sr anomalies and minor Eu anomalies, indicating no fractional crystallization of plagioclase. Significant Sr anomalies and modest Eu anomalies in Group 2 basalts indicate minor fractional plagioclase crystallization. Collectively, clinopyroxene and olivine were the primary components of the Group 1 basalts' crystal fractionation, whereas olivine, clinopyroxene, and plagioclase were the key components of the Group 2 basalts' crystal fractionation (Figure 9). These are consistent with the petrographic features as well (Figure 3).

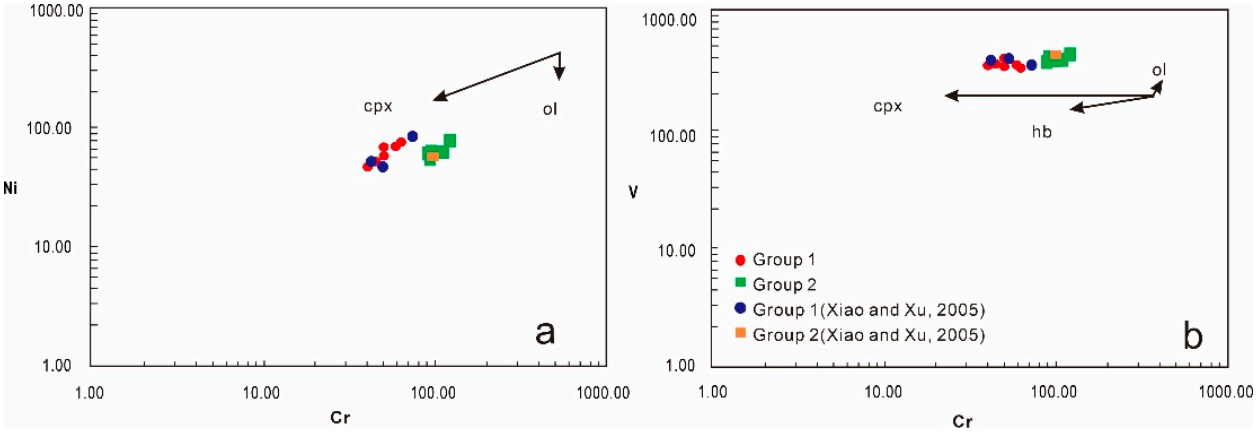


Figure 9. (**a**) Cr vs. Ni diagram; (**b**) Cr vs. V diagram [64].

5.1.2. Crustal Contamination

Crustal contamination of basalts is expected when the materials show that considerable volumes of melts have penetrated a continental crust [65]. According to previous researchers, the ratios of certain incompatible elements can be used to demonstrate crustal contamination [66–68]. For Dashibao basalt in the Xindianzi area, the Nb/Th ratios (Group 1 of 7.5–8.4 and Group 2 of 7.9–9.8) higher than those of the crust values (Nb/Th of 6.2) [68] reveal the predominant signature of mantle sources without considerable crustal contamination (Figure 10). Another key indicator of the continental crust is the depletion of Nb and Ta [59,69]. The contribution attributed to the upper crustal can be disregarded since Group 1 basalt patterns lack low Nb, Ta, and Ti negative anomalies (Figure 7). However, certain Group 2 basalts show Nb, Ta, and Ti depletion, suggesting that components of the lithospheric mantle were involved in the formation of the Group 2 magmas (Figure 7) [59,69]. The $(Th/Yb)_P$ ratio (normalized to primitive mantle), which reveals the importance of the Nb anomaly, is used to determine the level of crustal contamination. To assess the contribution of crustal pollution, the $(Nb/Th)_{PM}$ vs. $(Th/Yb)_{PM}$ diagram is often utilized [16,68]. Almost all of the Dashibao basalts in the Xindianzi area are in the field of the ELIP basalts, while all of the basalts are close to the Emeishan picrites. The Group 1 basalts are far from the upper crust domain (Figure 10). These features indicate negligible crustal contamination during the magma evolution. Group 2 basalts are plotted in the field between the primitive mantle and lower crust but are closer to the primitive mantle, implying minor crustal contamination [16] (Figure 10). In general, the evidence described above indicates that Group 1 basalts have no crustal contamination and Group 2 basalts are probably slightly modified by lower crust, which is consistent with the features of ELIP basalts [16,20,28,44]. Weak correlations between the SiO_2 and Nd isotopic compositions and no obvious linear relationship between the La/Nb rations and SiO_2 concentration (figure not shown in this paper) are evident in the Dashibao basalts of the Xindianzi area. Consequently, fractional crystallization (AFC) and assimilation are not considered to have played a significant role in the formation of the basalts [28].

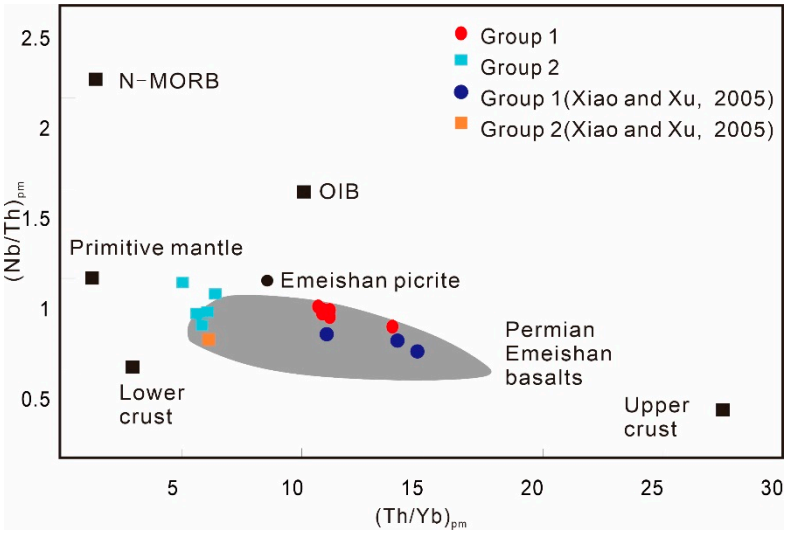


Figure 10. Crustal contamination discrimination diagrams for Dashibao basalts in the Xindianzi area. $(Nb/Th)_P$ vs. $(Th/Yb)_P$ plot is from [16].

5.1.3. Tectonic Setting

Continental flood basalts with geochemical features analogous to oceanic island basalts may be attributed to a mantle plume [2,21,47,70–73], and the geochemical characteristics, eruption period, and rock type of ELIP basalt suggest a mantle-plume origin of the Dashibao basalt in the Xindianzi area. Numerous geochemical and geophysical studies show that the partial melting degree of lavas is strongly influenced by the melting depth [16,74,75]. The degree of partial melting from Group 1 to Group 2 increases significantly in the Nb/Yb vs. Th/Yb plot [16] (Figure 11a). The La/Yb versus Sm/Yb diagram, which is very effective for distinguishing the origin of mafic magma [76–78], enables distinguishing between the melting of spinel and garnet peridotite. Figure 11b indicates that different degrees (5%–19%) of batch melting of a hypothetical light REE-enriched mantle source ((La/Yb) > 1) in the garnet stability field can generate La/Yb-Sm/Yb ratios similar to that of the Dashibao basalts. Group 1 HTi basalts could have originated from 8% to 10% melting of garnet peridotite. whereas Group 2 LTi basalts could have formed from 15% to 16% melting of garnet peridotite. Because the melting depth and degree are inversely related [79] and because the partial melting of the asthenospheric mantle brought on by a mantle plume may be the source of the magma of Group 1. The comparatively low degree of fractionation between HREE and LREE in Group 2 may reflect a higher degree of melting and a shallower source than Group 1 lavas.

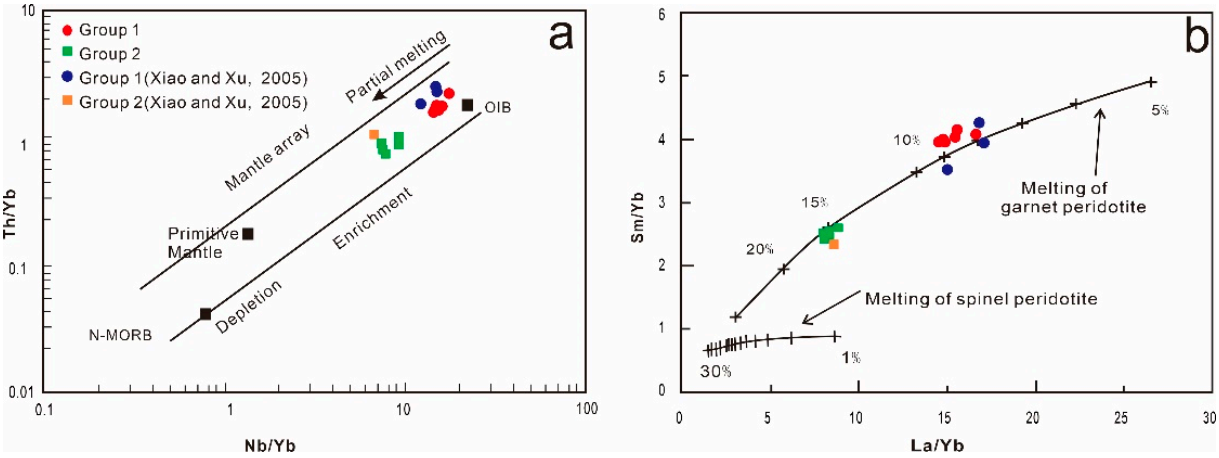


Figure 11. (**a**) Nb/Yb vs. Th/Yb diagram [16]; (**b**) Sm/Yb vs. La/Yb plot for Dashibao basalts in the Xindianzi area [80].

In the Zr/Y-Zr diagram [46], both Group 1 and Group 2 basalts are plotted in the within-plate basalts field (Figure 12a). In addition to the Th/Hf-Ta/Hf diagram [47] (Figure 12b), the Group 1 basalts are all plotted in the field of IV2 (intracontinental rift alkali basalts), while the Group 2 basalts are all plotted in the field of IV1 (intracontinental rift + continental margin rift tholeiites). The within-plate nature of the Dashibao basalts suggests that these rocks may be formed in a continental rift or a back-arc basin [80]. Zr/Y (6.9–10.6) and Zr/Sm (28–33) ratios are similar to those found in many intra-plate basalts (Zr/Y > 3.5, Zr/Sm≈30) (Figure 11a) [61], but differ from those found in island arc rocks (Zr/Y < 33.5, Zr/Sm≈20) [61,63]. Therefore, the above results suggest that the Dashibao basalts in the Xindianzi area were formed in an extension-related within-plate environment.

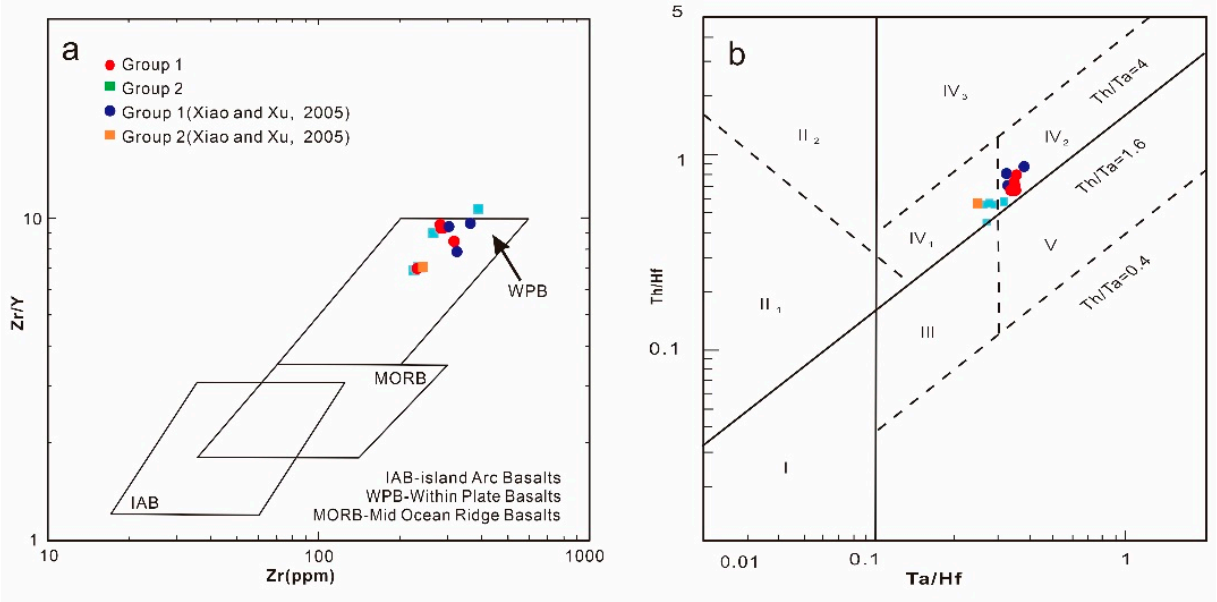


Figure 12. Tectonic discrimination diagrams for Dashibao basalt in the Xindianzi area. (**a**) Zr/Y-Zr [46], (**b**) Ta/Hf–Th/Hf diagram [47]. I. Plate divergent margin MORB; II1. Ocean island-arc basalts; II2. Continental margin island-arc + continental margin volcanic-arc basalts; III. Oceanic within-plate basalts; IV1. Intracontinental rift + continental margin rift tholeiites; IV2. Intracontinental rift alkali basalts; IV3. Continental extensional zone/initial rift basalts; V. Mantle plume basalts.

5.2. Chemostratigraphic Comparison of Late Permian Basalts

The Permian basalts were divided into the Gangdagai Formation in the Zhongza Terrane and the Ganzi–Litang Terrane and the Dashibao Formation in the SGT [42]. The basalts have thicknesses varying from tens of meters (Xindianzi) to four thousand meters (Sanjiangkou), all have LTi or HTi rock association, which is part of the Emeishan basalt. To compare the chemical stratigraphy of Zhongzan, Ganzi-Litang, Songpan–Ganzi and Emeishan basalts, six representative volcanic sequences on the western and eastern sides of the Longmenshan fault zone were established. Geochemical features allowed the distinction between high-titanium (HTi, TiO_2 > 2.5 wt%; Ti/Y > 500) and low-titanium basalts (LTi, TiO_2 < 2.5 wt%: Ti/Y < 500) [20,44]. Results reveal that Sanjiangkou, Baoxing, and Xindianzi areas are all characterized by LTi basalt at the bottom and HTi basalt on top, a similar sequence may be observed at Binchuan (Figure 13).

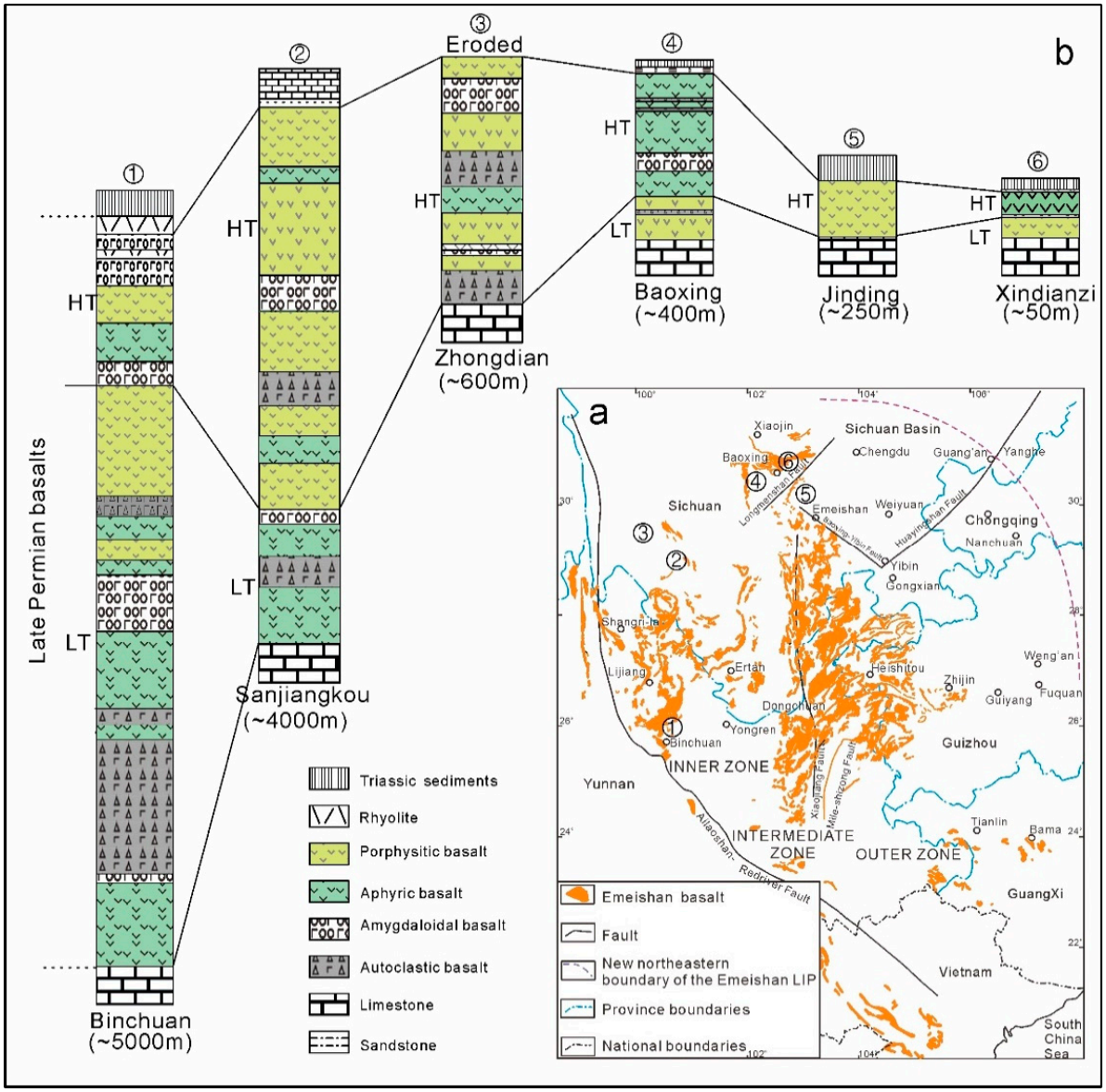


Figure 13. (**a**) Geological sketch map showing the area of the ELIP [60]. (**b**) Representative stratigraphic columns of Emeishan basalts [15,25,28,40,42,44,60,81].

Previous studies have proven that the Zhongzan Terrane and SGT are both parts of the South China Block and were disconnected from the South China Block in the Late Permian [26,40,81]. The current distribution may be due to the Late Permian-Triassic splitting of South China Block separating Emeishan basalts in two unequal parts. This is testified by the stratigraphic and geochemical correlation of lavas of the Zhongzan Terrane, SGT, and Ganzi-Litang Terrane [81].

5.3. Eruption of Bashibao Basalts

The age of the ELIP has been generally constrained at about 260 Ma by zircon U–Pb dating of mafic intrusions and some felsic plutons [45,82–84]. Due to the influence of metamorphism, the age of Dashibao Basalts was only constrained by the regional stratigraphic relationships and only a few dating results, including SHRIMP U-Pb zircon ages of 263 ± 2.0 Ma [28] and 257.3 ± 2.0 Ma [16] (Figure 1a).

In this paper, we collected samples and separated zircons of the Dashibao basalts and their overlying tuffs along Sections 1 and 2 in the Xindianzi area (Figure 4). Three new dating results were obtained by SIMS zircon U-Pb method. Basalt sample XDZ02-

1 was dated at 259.1 ± 1.66 Ma, and tuff samples XC05-2 and XDZ05-1 were dated at 251.5 ± 0.27 Ma and 251.8 ± 1.57 Ma, respectively. The age of the basalts is consistent with the main ELIP eruption period at approximately 260 million years ago, suggesting a close genetic connection between the Dashibao basalts and the ELIP flood basalts [16,26,28,29].

Tuff layers could be considered a stratigraphic marker to establish the temporal framework with high-precision geochronology [28,85–88]. Thus, the tuffs that form the uppermost part of the Dashibao basalts (XC05-2 and XDZ05-1) constrain the termination of volcanism of the Dashibao basalts at 251 Ma (Figure 3c). The previous SHRIMP U-Pb zircon age of 263 ± 2.0 Ma from the Dashibao basalts in Xindianzi area might represent the initial eruption time [28] (Figure 1b). Therefore, the ELIP eruption of the Dashibao basalts in the Songpan–Ganzi area could be constrained between 263 May and 251 Ma with ~10 Ma duration for the entire eruptive phase of the flood basalts.

5.4. Duration and End of the ELIP Magmatism

The Dashibao basalts in Songpan–Ganzi have an affinity with the ELIP basalts [16,26,28,89], and their age creates a certain inference in terms of the end of the ELIP. Numerous studies have currently defined the age and duration of the ELIP. Despite more than 200 radiometric ages ranging from 235 to 271 Ma [17,82,84,90,91], there is still considerable debate regarding the end of the ELIP volcanism. Boven et al. (2002), Lo et al. (2002), and Fan et al. (2004) [92–94] obtained $^{40}Ar/^{39}Ar$ ages ranging from 253 Ma to 251 Ma in the Baise area, indicating that ELIP magmatism probably ceased between 253 and 251 Ma. Unfortunately, due to post-eruption alteration and thermotectonic resetting of the basalts, the $^{40}Ar/^{39}Ar$ isotopic dating technique proved inapplicable for the ELIP [94,95]. Therefore, the 40Ar/39Ar ages have been questioned [95,96]. He et al. (2007) [97] obtained zircon U-Pb ages of 263 ± 5 Ma and 257 ± 3 Ma for welded tuff at the top of the ELIP basalt section in Pu'eryuan, Yunnan Province, and the clastic rocks of Xuanwei Formation in the eastern Pu'er area, suggesting that the ELIP basalts erupted at ~263 Ma and ended before the deposition of the Xuanwei Formation at 257 ± 3 Ma. However, the measured samples have a large error, with MSWDs of 7.5 and 6.5. Moreover, detrital zircons from the sedimentary rocks at the bottom of the Xuanwei Formation do not necessarily come from the ELIP basalts, and the welded tuff samples are also not taken from the top of the section [82]. Shellnutt (2008) [98] obtained SHRIMP zircon ages of 252 ± 2.5 Ma and 251 ± 6 Ma for the Huangcao and Ailanghe plutons in the Panxi region. This is the first indication from the plutonic rocks that the ELIP magmatism may have continued into the Late Permian. Subsequently, Zhu et al. (2011) [99] obtained a zircon U-Pb age of 251.0 ± 1.0 Ma for a tuff unit from the uppermost part of the ELIP basalt in Panxian, Guizhou province; Wang et al. (2018) [100] obtained a SHRIMP zircon U–Pb age of 251.9 ± 0.037 Ma from coal beds close to the end-Permian mass in the eastern Yunnan Province; and in the Wude ELIP basalt, a U-Pb age of 251.3 ± 2.0 Ma was obtained, consistent with our new tuff dating results. Therefore, we suggest that 251 Ma represents the end of ELIP volcanism, which occurred roughly when the Siberian Traps' principal eruption occurred [18,101,102]. This new age result matches the age of the P-T boundary in southern China [103]. Thus, we conclude that 251 Ma mark the end of the ELIP. The eruption duration of ELIP basalt may exceed 10 Ma.

5.5. Continental Breakup and ELIP Mantle Plume

Continental flood basalt brought by mantle plumes or super-plumes contributes to re constructing the supercontinent framework [12,104–109]. Intraplate magmatism spans the entire spectrum, from widespread subalkaline flood basalt provinces to rift volcanism with more alkaline provinces [61]. As a result, our comparison of the geochemical fingerprints of key magmatic events, as well as the lithostratigraphy of contemporary rift sequences helps in the reconstruction of ancient continental masses [64,104,106].

Studies of petrology, geochemistry, biostratigraphy, and geochronology provide evidence for the affinity between the South China Block and the SGT [13,14,25,33] (Figure 1). As shown in Figure 1: (1) the Neoproterozoic granitic gneiss and metavolcanic rocks in the southeast margin of the SGT are comparable to the Neoproterozoic basement of the western margin of the South China block in terms of petrology and geochemistry [13,14,26,28].

(2) The thick Sinian–Lower Permian continental margin shallow-to deep-marine clastic and carbonate sedimentary rocks in the southeastern margin of the SGT are similar to the Sinian Lower Permian shallow-marine clastic sedimentary rocks and carbonate rocks in the western part of the South China block. (3) The same Ordovician to lower Permian fossils are found in the sedimentary rocks of both regions. Therefore, similar sedimentary sequences and the same fossils in the two tectonic blocks show that the Late Mesoproterozoic to Paleozoic strata and their flora and fauna in the SGT are equivalent to those in the South China block, and they were thought to have affinity before the Late Permian [25,26,110,111].

In the Permian, sediments characteristic of extensional environments, such as car bonate gravity flow, turbidite, and siliceous rocks, were widely deposited along the NW margin of the South China Block [112–116]. The Lower Permian strata in the eastern margin of the Songpan-Garzi fold belt are composed of deep-water shale, sandstone, and limestone, often containing exotic limestone–gravel clumps. Some clastic rocks show the characteristics of turbidite, reworked from the continental shelf and accumulated in deep water [112,116]. The interbedding of conglomerate layers and chaotic limestone layers following platform sediments in the stratigraphic sequence suggests syn-sedimentary tectonics and deepening coeval with the eruption of pillow lavas. The existence of the high-density and high-resistivity mafic and ultra-mafic shallow materials in the lithosphere near the Longmen Shan Tectonic belt also reveals that extensional rupture of the lithosphere and massive upwelling of mantle material occurred in this area [117]. During the Late Permian, the Longmen Shan tectonic belt on the margin of the Songpan–Ganzi Terrane and South China Block underwent rifting, accompanied by extensive magmatism [118].

Mantle plume activity can cause regional uplift, lithosphere extension, and thinning, producing massive amounts of magma by decompression melting. Although the role of mantle plume activity in continental breakup or the mode of participation (active or passive, or both) remains controversial, it is at least involved in continental breakup [3,11,105,119–121]. This paper proposes a rift driven by a mantle plume with the following evidence: (1) the ELIP mantle plume has been widely recognized [15,20,42,122–125]; (2) The unconformity between the lower Permian limestone or marble of the South China Block and the ELIP continental flood basalt indicates that the lithosphere in the western margin of the South China Block was widely uplifted before basalt eruption [15,21,122,126,127]. This implies that a sequential process of lithosphere extension and thinning, mantle plume gushing upward, and a huge amount of magma produced by rapid decompression melting led to large-scale volcanism and suggests that continental breakup was a response to the Late Permian ELIP plume; (3) The seismo-megaturbidite, which may reflect rifting and slope creation induced by the Emeishan mantle plume, was formed in submarine collapse slope facies at the base of the Sandaoqiao formation in the Baoxing area. (Figure 11) [16,25,128]; in previous studies, the regional stratigraphic sequence also reflects the rift environment characterized by lithospheric stretching [124]. (4) At about 260 Ma, the ELIP basalt eruption coincided with the rifting of the western margin of the South China Block. Flood basalt volcanism with large plumes and rifting are precisely correlated in both space and time [3]. It seems unlikely that this exact correspondence is just a coincidence.

5.6. The Rift in the Southeastern Margin of the Songpan–Ganzi Terrane?

Many authors have proposed that the west of the South China Block is the site of an ancient triple junction [16,25,26,28,39,129,130]. Among them are, the northwest branch and the south branch separated from the Permian to the Triassic, forming a new oceanic crust and becoming part of the eastern Tethys Ocean. The northeastern branch located between the Longmen Shan tectonic belt and the Songpan-Garzi Terrane, is an abandoned branch that was not oceanized (Figure 14b) [39,131].

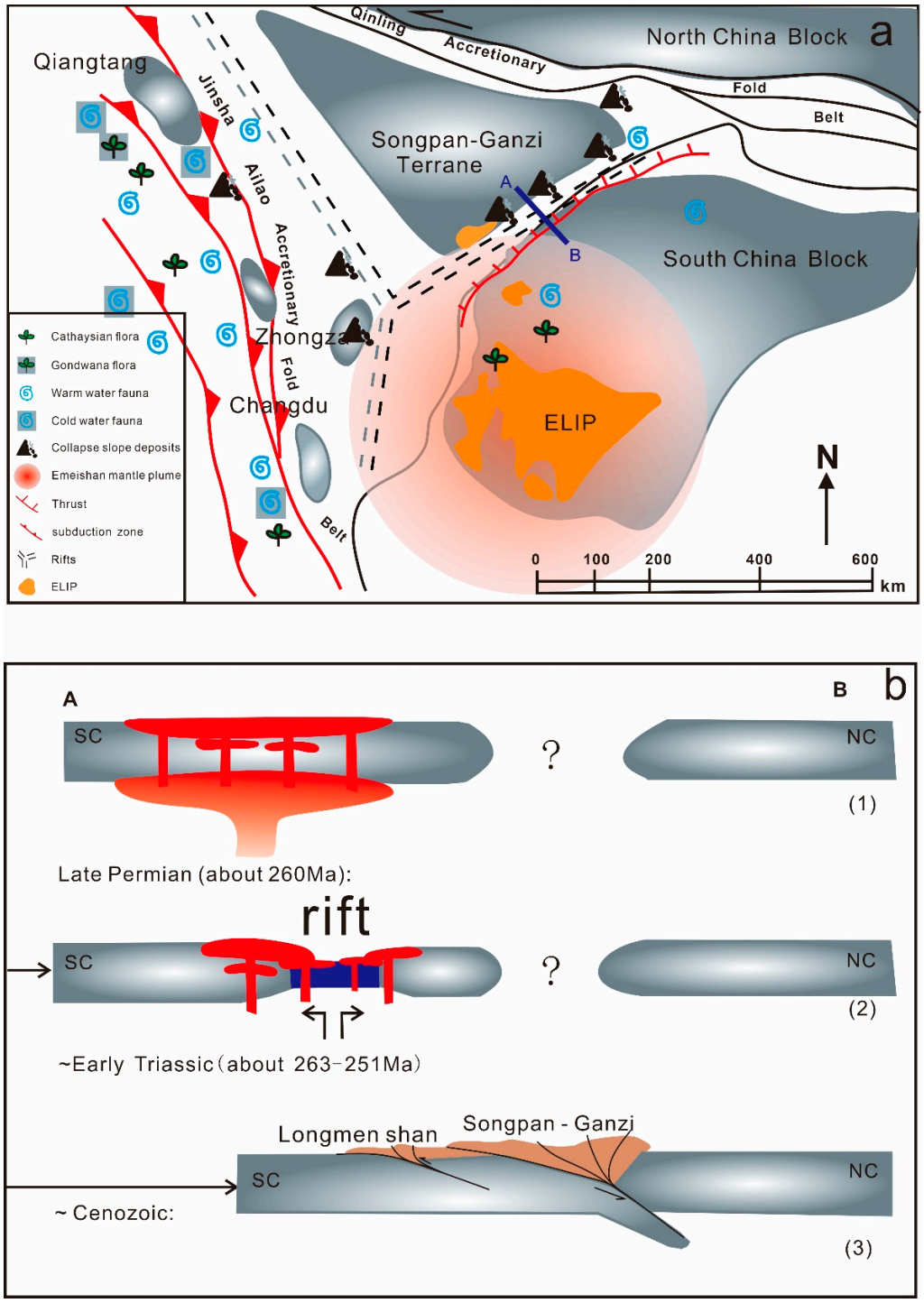


Figure 14. (**a**) Cartoon showing the Permian–Triassic triple junction of continental rifts (RRR) developed in the Songpan–Ganzi Terrane (modified from [16,25]. AB: location of evolutionary sections of b. (**b**) Cartoons illustrating the tectonic evolution of northwest margin of the South China Block from Late Permian to Cenozoic: (1) Late Permian (about 260 Ma): mantle plume within the South China Block; (2) Early Triassic(about 263–251 Ma): the mantle plume triggers the separation of the SGT; (3) ~Cenozoic: Finally, the subduction and collision of the South China Block and North China Block, which produced extensive thrust nappe in southeastern margin of the SGT, strike–slip faults along the Longmen Shan tectonic belt, and a significant amount of thrust faulting and folding eventually overwhelmed the rift system and the rift finally closed. SC. South China Block, NC. North China Block.

This article reports, for the first time the geochemistry, petrology, and geochronology of the intraplate basalts in the syn-rift period, and thus shed new lights on the origin of the Songpan–Ganzi Terrane.

When the Late Permian ELIP mantle plume arrived close to the base of the lithosphere at about 260 Ma, it caused flood basalt volcanism. With the continuation of volcanism, the lithosphere was extended, and rifting occurred. The dissipation of thermal and mechanical energy at the head of the plume resulted in strong but short-duration rifting and magmatism. As the plume head spreads beneath the lithosphere, the ELIP mantle plume triggered the formation of a Rift–Rift–Rift (RRR) triple junction on the western margin of the South China Block (Figure 14b).

The northwest and south branches split and formed a new oceanic crust to become part of the eastern Tethys in the Late Permian. The other branch is located in the southeastern margin of the SGT, due to the subduction and collision of the South China Block and North China Block and the closure of the Paleo-Tethys Ocean, which sealed off the development of this branch, prevented complete continental separation, and produced extensive thrust tectonics in the southeastern margin of the SGT and strike–slip faults along the Longmen Shan tectonic belt (Figure 14a) [31,39,118]. After the end of extension and volcanism, thrust faulting and folding eventually overwhelmed the rift system and the rift finally closed.

6. Conclusions

(1) The Dashibao basalts in the Xindianzi area include alkaline (HTi) and continental flood basalts (LTi) that erupted during the Late Permian in a continental rift located at the periphery of the ELIP mantle plume. Dashibao basalts in the marginal area of the ELIP mantle plume erupted in a continental rift setting in the Late Permian.

(2) Dashibao basalts dated at 259 Ma by SIMS zircon U-Pb, are coeval with the ELIP magmatism. Dating results of tuff zircons from the top of the Dashibao basalts constrain the termination of Dashibao basalts at 251.8 $\pm$ 1.57 Ma, and thus, eruption of the Dashibao basalts occurred at intervals of ~10 Ma from 259 to 251 Ma.

(3) The ELIP mantle plume formed an RRR triple junction in the western margin of the South China Block. The northwest branch and the south branch of rifts spread and formed a new oceanic crust in the eastern Tethys. The northeastern branch rift located between the Longmen Shan thrust belt and Songpan–Ganzi terrane was finally closed by subsequent top-to-south imbricate thrust when the South China Block was subducted beneath the North China Block.

Supplementary Materials: The following supporting information can be downloaded at: https://www.mdpi.com/article/10.3390/min12111391/s1, Table S1: Zircon SIMS U–Pb analytical data of xindianzi basalts and Xuecheng tuff.; Table S2: Major oxides and trace elements for Dashibao basalts in the Xindianzi area.; Table S3: Sr-Nd isotopes of Xindianzi basalts. Method S1: Analytical methods.

Author Contributions: Page: 19Conceptualization, D.Y. and Y.S.; validation, Y.S., D.Y. and L.Q.; formal analysis, Y.S.; investigation, Y.S., D.Y., L.Q., H.M. and Y.Z.; data curation, Y.S.; writing—original draft preparation, Y.S.; writing—review and editing, Y.S., D.Y and L.Q.; visualization, Y.S.; supervision, D.Y. All authors have read and agreed to the published version of the manuscript.

Funding: This research was funded by the National Natural Science Foundation of China (42030306), and the Fundamental Research Funds for the Central Universities (292019046).

Data Availability Statement: All data used in this study are freely available.

Acknowledgments: We express our thanks to anonymous reviewers for their constructive comments, which significantly improved the manuscript.

Conflicts of Interest: The authors declare no conflict of interest.

References

1. Bryan, S.E.; Ernst, R.E. Revised definition of Large Igneous Provinces (LIPs). *Earth Sci. Rev.* **2008**, *86*, 175–202. [CrossRef]
2. Coffin, M.; Eldholm, O. Large igneous provinces: Crustal structure, dimensions, and external consequences. *Rev. Geophys.* **1994**, *32*, 1–36. [CrossRef]
3. Courtillot, V.; Jaupart, C.; Manighetti, I.; Tapponnier, P.; Besse, J. On causal links between flood basalts and continental breakup. *Earth Planet. Sci. Lett.* **1999**, *166*, 177–195. [CrossRef]
4. Encarnacion, J.; Grunow, A. Changing magmatic and tectonic styles along the paleo-Pacific margin of Gondwana and the onset of early Paleozoic magmatism in Antarctica. *Tectonics* **1996**, *15*, 1325–1341. [CrossRef]
5. Jolley, D.W.; Bell, B.R. The evolution of the North Atlantic Igneous Province and the opening of the NE Atlantic rift. *Geol. Soc. Lond. Spéc. Publ.* **2002**, *197*, 1–13. [CrossRef]
6. Jourdan, F.; Féraud, G.; Bertrand, H.; Watkeys, M.; Kampunzu, A.; Le Gall, B. Basement control on dyke distribution in Large Igneous Provinces: Case study of the Karoo triple junction. *Earth Planet. Sci. Lett.* **2006**, *241*, 307–322. [CrossRef]
7. Morgan, W.J. Convection Plumes in the Lower Mantle. *Nature* **1971**, *230*, 42–43. [CrossRef]
8. Nikishin, A.; Ziegler, P.; Abbott, D.; Brunet, M.-F.; Cloetingh, S. Permo–Triassic intraplate magmatism and rifting in Eurasia: Implications for mantle plumes and mantle dynamics. *Tectonophysics* **2002**, *351*, 3–39. [CrossRef]
9. Reeves, C.; De Wit, M. Making ends meet in Gondwana: Retracing the transforms of the Indian Ocean and reconnecting continental shear zones. *Terra Nova* **2000**, *12*, 272–280. [CrossRef]
10. Storey, B.C.; Alabaster, T.; Hole, M.J.; Pankhurst, R.J.; Wever, H.E. Role of subduction-plate boundary forces during the initial stages of Gondwana break-up: Evidence from the proto-Pacific margin of Antarctica. *Geol. Soc. Lond. Spéc. Publ.* **1992**, *68*, 149–163. [CrossRef]
11. Storey, B.C. The role of mantle plumes in continental breakup: Case histories from Gondwanaland. *Nature* **1995**, *377*, 301–308. [CrossRef]
12. White, R.S.; McKenzie, D.P. Volcanism at rifts. *Sci. Am.* **1989**, *261*, 62–71. [CrossRef]
13. Sichuan BGMR. *Regional Geological Report of Guanxian at the Scale of 1:200,000*; Geological Publishing House: Beijing, China, 1975.
14. Sichuan BGMR. *Bureau of Geology and Mineral Resources of Sichuan Province Regional geology of Sichuan Province*; Geological Publishing House: Beijing, China, 1976.
15. He, B.; Xu, Y.; Xiao, L.; Wang, K.; Sha, S. Generation and Spatial Distribution of the Emeishan Large Igneous Province: New Evidence from Stratigraphic Records. *Acta Geol. Sin.* **2003**, *77*, 194–202.
16. Li, H.; Zhang, Z.; Santosh, M.; Lü, L.; Han, L.; Liu, W.; Cheng, Z. Late Permian basalts in the northwestern margin of the Emeishan Large Igneous Province: Implications for the origin of the Songpan-Ganzi terrane. *Lithos* **2016**, *256–257*, 75–87. [CrossRef]
17. Li, M.; Yang, B.; Qiu, L.; Zhang, Y.; Xu, H.; Shi, X.; Tian, W.; Wang, Y.; Gao, J.; Zheng, D. Emeishan felsic volcanism lasted until the Changhsingian? New evidence from volcanic ash in the northern South China block. *J. Southeast Asian Earth Sci.* **2022**, *238*, 105390. [CrossRef]
18. Shellnutt, J.G.; Denyszyn, S.W.; Mundil, R. Precise age determination of mafic and felsic intrusive rocks from the Permian Emeishan large igneous province (SW China). *Gondwana Res.* **2012**, *22*, 118–126. [CrossRef]
19. Shellnutt, J.G.; Zhou, M.-F. Permian, rifting related fayalite syenite in the Panxi region, SW China. *Lithos* **2008**, *101*, 54–73. [CrossRef]
20. Xu, Y.; Chung, S.-L.; Jahn, B.-M.; Wu, G. Petrologic and geochemical constraints on the petrogenesis of Permian–Triassic Emeishan flood basalts in southwestern China. *Lithos* **2001**, *58*, 145–168. [CrossRef]
21. Xu, Y.-G.; He, B.; Chung, S.-L.; Menzies, M.; Frey, F.A. Geologic, geochemical, and geophysical consequences of plume involvement in the Emeishan flood-basalt province. *Geology* **2004**, *32*, 917. [CrossRef]
22. Xu, Y.-G.; Luo, Z.-Y.; Huang, X.-L.; He, B.; Xiao, L.; Xie, L.-W.; Shi, Y.-R. Zircon U–Pb and Hf isotope constraints on crustal melting associated with the Emeishan mantle plume. *Geochim. Et Cosmochim. Acta* **2008**, *72*, 3084–3104. [CrossRef]
23. Zhang, Z.; Mao, J.; Saunders, A.D.; Yu, A.; Ying, L.; Li, Z. Petrogenetic modeling of three mafic–ultramafic layered intrusions in the Emeishan large igneous province, SW China, based on isotopic and bulk chemical constraints. *Lithos* **2009**, *113*, 369–392. [CrossRef]
24. Ali, J.R.; Fitton, J.; Herzberg, C. Emeishan large igneous province (SW China) and the mantle-plume up-doming hypothesis. *J. Geol. Soc.* **2010**, *167*, 953–959. [CrossRef]
25. Chang, E.Z. Geology and Tectonics of the Songpan-Ganzi Fold Belt, Southwestern China. *Int. Geol. Rev.* **2000**, *42*, 813–831. [CrossRef]
26. Song, X.-Y.; Zhou, M.-F.; Cao, Z.-M.; Robinson, P.T. Late Permian rifting of the South China Craton caused by the Emeishan mantle plume? *J. Geol. Soc.* **2004**, *161*, 773–781. [CrossRef]
27. Zi, J.; Fan, W.; Wang, Y.; Peng, T.; Guo, F. Geochemistry and petrogenesis of the Permian mafic dykes in the Panxi region, SW China. *Gondwana Res.* **2008**, *14*, 368–382. [CrossRef]
28. Zi, J.-W.; Fan, W.-M.; Wang, Y.-J.; Cawood, P.A.; Peng, T.-P.; Sun, L.-H.; Xu, Z.-Q. U-Pb geochronology and geochemistry of the Dashibao Basalts in the Songpan-Ganzi Terrane, SW China, with implications for the age of Emeishan volcanism. *Am. J. Sci.* **2010**, *310*, 1054–1080. [CrossRef]
29. Xiao, L.; Xu, J. Petrogenesis and tectonic setting of Dashibao Group basalts from Songpan-Ganze block, northwestern Sicuan province, China. *Acta Petrol.* **2005**, *21*, 1539–1545.

30. Zhang, K. Is the Songpan-Ganzi terrane (central China) really underlain by oceanic crust? *J.-Geol. Soc. India* **2001**, *57*, 223–230.
31. Burchfiel, B.C.; Zhiliang, C.; Yupinc, L.; Royden, L.H. Tectonics of the Longmen Shan and Adjacent Regions, Central China. *Int. Geol. Rev.* **1995**, *37*, 661–735. [CrossRef]
32. Guo, X.; Gao, R.; Xu, X.; Keller, G.R.; Yin, A.; Xiong, X. Longriba fault zone in eastern Tibet: An important tectonic boundary marking the westernmost edge of the Yangtze block. *Tectonics* **2015**, *34*, 970–985. [CrossRef]
33. Roger, F.; Malavieille, J.; Leloup, P.; Calassou, S.; Xu, Z. Timing of granite emplacement and cooling in the Songpan–Garzê Fold Belt (eastern Tibetan Plateau) with tectonic implications. *J. Southeast Asian Earth Sci.* **2004**, *22*, 465–481. [CrossRef]
34. Xiao, L.; Zhang, H.; Clemens, J.; Wang, Q.; Kan, Z.; Wang, K.; Ni, P.; Liu, X. Late Triassic granitoids of the eastern margin of the Tibetan Plateau: Geochronology, petrogenesis and implications for tectonic evolution. *Lithos* **2007**, *96*, 436–452. [CrossRef]
35. Zhang, H.-F.; Zhang, L.; Harris, N.; Jin, L.-L.; Yuan, H. U–Pb zircon ages, geochemical and isotopic compositions of granitoids in Songpan-Garze fold belt, eastern Tibetan Plateau: Constraints on petrogenesis and tectonic evolution of the basement. *Contrib. Miner. Pet.* **2006**, *152*, 75–88. [CrossRef]
36. Bruguier, O.; Lancelot, J.; Malavieille, J. U–Pb dating on single detrital zircon grains from the Triassic Songpan–Ganze flysch (Central China): Provenance and tectonic correlations. *Earth Planet. Sci. Lett.* **1997**, *152*, 217–231. [CrossRef]
37. Zhou, D.; Graham, S. The Songpan-Ganzi complex of the West Qinling Shan as a Triassic remnant ocean basin. *World Reg. Geol.* **1996**, *1*, 281–299.
38. Sengör, A.M.C.; Natal'In, B.A. Turkic-type orogeny and its role in the making of the continental crust. *Annu. Rev. Earth Planet. Sci.* **1996**, *24*, 263–337. [CrossRef]
39. Yan, D.-P.; Zhou, Y.; Qiu, L.; Wells, M.L.; Mu, H.; Xu, C.-G. The Longmenshan Tectonic Complex and adjacent tectonic units in the eastern margin of the Tibetan Plateau: A review. *J. Southeast Asian Earth Sci.* **2018**, *164*, 33–57. [CrossRef]
40. Chung, S.-L.; Jahn, B.-M. Plume-lithosphere interaction in generation of the Emeishan flood basalts at the Permian-Triassic boundary. *Geology* **1995**, *23*, 889. [CrossRef]
41. Liu, J.; Nechaev, V.P.; Dai, S.; Song, H.; Nechaeva, E.V.; Jiang, Y.; Graham, I.T.; French, D.; Yang, P.; Hower, J.C. Evidence for multiple sources for inorganic components in the Tucheng coal deposit, western Guizhou, China and the lack of critical-elements. *Int. J. Coal Geol.* **2020**, *223*, 103468. [CrossRef]
42. Xiao, L.; Xu, Y.; Mei, H.; Zheng, Y.-F.; He, B.; Pirajno, F. Distinct mantle sources of low-Ti and high-Ti basalts from the western Emeishan large igneous province, SW China: Implications for plume–lithosphere interaction. *Earth Planet. Sci. Lett.* **2004**, *228*, 525–546. [CrossRef]
43. Song, X.-Y.; Zhou, M.-F.; Hou, Z.-Q.; Cao, Z.-M.; Wang, Y.-L.; Li, Y. Geochemical Constraints on the Mantle Source of the Upper Permian Emeishan Continental Flood Basalts, Southwestern China. *Int. Geol. Rev.* **2001**, *43*, 213–225. [CrossRef]
44. Xiao, L.; Xu, Y.-G.; Chung, S.-L.; He, B.; Mei, H. Chemostratigraphic Correlation of Upper Permian Lavas from Yunnan Province, China: Extent of the Emeishan Large Igneous Province. *Int. Geol. Rev.* **2003**, *45*, 753–766. [CrossRef]
45. Zhou, M.-F.; Malpas, J.; Song, X.-Y.; Robinson, P.T.; Sun, M.; Kennedy, A.K.; Lesher, C.; Keays, R.R. A temporal link between the Emeishan large igneous province (SW China) and the end-Guadalupian mass extinction. *Earth Planet. Sci. Lett.* **2002**, *196*, 113–122. [CrossRef]
46. Pearce, J.A.; Norry, M.J. Petrogenetic implications of Ti, Zr, Y, and Nb variations in volcanic rocks. *Contrib. Mineral. Petrol.* **1979**, *69*, 33–47. [CrossRef]
47. Yunliang, W.; Chengjiang, Z.; Shuzhi, X. Th/Hf-Ta/Hf identification of tectonic setting of basalts. *Acta Petrol. Sin.* **2001**, *17*, 413–421.
48. He, S.; Li, Z.; Al Jehani, A.; Guo, D.; Harbi, Z.; Zhang, Y. Nb–Ta Behaviour during Magma-to-Pegmatite Transformation Process: Record from Zircon Megacrysts in Pegmatite. *Minerals* **2021**, *11*, 1139. [CrossRef]
49. Su, L.; Song, S.; Wang, C.; Allen, M.B.; Zhang, H. Picrite-basalt complex in the Baoshan-Gongshan Block of northern Sibumasu: Onset of a mantle plume before breakup of Gondwana and opening of the Neo-Tethys Ocean. *GSA Bull.* **2022**, *134*, 1091–1108. [CrossRef]
50. DuFrane, S.A.; Turner, S.; Dosseto, A.; van Soest, M. Reappraisal of fluid and sediment contributions to Lesser Antilles magmas. *Chem. Geol.* **2009**, *265*, 272–278. [CrossRef]
51. Li, C.-F.; Chen, F.; Li, X.-H. Precise isotopic measurements of sub-nanogram Nd of standard reference material by thermal ionization mass spectrometry using the NdO+ technique. *Int. J. Mass Spectrom.* **2007**, *266*, 34–41. [CrossRef]
52. Wiesmaier, S.; Deegan, F.M.; Troll, V.R.; Carracedo, J.C.; Chadwick, J.P.; Chew, D.M. Magma mixing in the 1100 AD Montaña Reventada composite lava flow, Tenerife, Canary Islands: Interaction between rift zone and central volcano plumbing systems. *Contrib. Miner. Pet.* **2011**, *162*, 651–669. [CrossRef]
53. Hoskin, P.; Black, L. Metamorphic zircon formation by solid-state recrystallization of protolith igneous zircon. *J. Metamorph. Geol.* **2000**, *18*, 423–439. [CrossRef]
54. Hoskin, P.W.O.; Schaltegger, U. The composition of zircon and igneous and metamorphic petrogenesis. *Rev. Mineral. Geochem.* **2003**, *53*, 27–62. [CrossRef]
55. Wu, Y.; Zheng, Y.-F. Genesis of zircon and its constraints on interpretation of U-Pb age. *Chin. Sci. Bull.* **2004**, *49*, 1554–1569. [CrossRef]
56. Miyashiro, A. Volcanic rock series and tectonic setting. *Annu. Rev. Earth Planet. Sci.* **1975**, *3*, 251. [CrossRef]

57. Winchester, J.A.; Floyd, P.A. Geochemical discrimination of different magma series and their differentiation products using immobile elements. *Chem. Geol.* **1977**, *20*, 325–343. [CrossRef]
58. Sun, S.S.; McDonough, W.F. Chemical and isotopic systematics of oceanic basalts: Implications for mantle composition and processes. In *Magmatism in the Ocean Basin*; Geological Society Special Publication: London, UK, 1989; Volume 42, pp. 313–345.
59. Frey, F.A.; Green, D.H.; Roy, S.D. Integrated Models of Basalt Petrogenesis: A Study of Quartz Tholeiites to Olivine Melilitites from South Eastern Australia Utilizing Geochemical and Experimental Petrological Data. *J. Pet.* **1978**, *19*, 463–513. [CrossRef]
60. Li, H.; Zhang, Z.; Santosh, M.; Lü, L.; Han, L.; Liu, W. Late Permian basalts in the Yanghe area, eastern Sichuan Province, SW China: Implications for the geodynamics of the Emeishan flood basalt province and Permian global mass extinction. *J. Southeast Asian Earth Sci.* **2017**, *134*, 293–308. [CrossRef]
61. Shellnutt, J.G. The Emeishan large igneous province: A synthesis. *Geosci. Front.* **2014**, *5*, 369–394. [CrossRef]
62. Wilson, M. *Igneous Petrogenesis*; Springer: Berlin/Heidelberg, Germany, 1989.
63. Arth, J.G. Behaviour of trace elements during magmatic processes. *US Geol. Surv. J. Res.* **1976**, *4*, 41–47.
64. Xu, X.; Song, S.; Su, L.; Li, Z.; Niu, Y.; Allen, M.B. The 600–580Ma continental rift basalts in North Qilian Shan, northwest China: Links between the Qilian-Qaidam block and SE Australia, and the reconstruction of East Gondwana. *Precambrian Res.* **2015**, *257*, 47–64. [CrossRef]
65. Reichow, M.K.; Saunders, A.; White, R.; Al'Mukhamedov, A.; Medvedev, A. Geochemistry and petrogenesis of basalts from the West Siberian Basin: An extension of the Permo–Triassic Siberian Traps, Russia. *Lithos* **2005**, *79*, 425–452. [CrossRef]
66. Neal, C.R.; Mahoney, J.J.; Iii, W.J.C. Mantle Sources and the Highly Variable Role of Continental Lithosphere in Basalt Petrogenesis of the Kerguelen Plateau and Broken Ridge LIP: Results from ODP Leg 183. *J. Pet.* **2002**, *43*, 1177–1205. [CrossRef]
67. Peng, Z.; Mahoney, J.; Hooper, P.; Harris, C.; Beane, J. A role for lower continental crust in flood basalt genesis? Isotopic and incompatible element study of the lower six formations of the western Deccan Traps. *Geochim. Et Cosmochim. Acta* **1994**, *58*, 267–288. [CrossRef]
68. Zhu, D.Y.; Lau, L.; Liu, S.H.; Wei, J.S.; Lu, Y.M. Activation of cAMP-response-element-binding protein (CREB) after focal cerebral ischemia stimulates neurogenesis in the adult dentate gyrus. *Proc. Natl. Acad. Sci. USA* **2004**, *101*, 9453–9457. [CrossRef] [PubMed]
69. Rudnick, R.; Gao, S.; Holland, H.; Turekian, K. Composition of the continental crust. *Crust* **2003**, *3*, 1–64.
70. Thompaon, A.; Willams, J. Age hardening in Cu-2.5 wt% Ti. *Metall. Trans. A* **1984**, *15*, 931–937. [CrossRef]
71. Campbell, I.H.; Griffiths, R.W. Implications of mantle plume structure for the evolution of flood basalts. *Earth Planet. Sci. Lett.* **1990**, *99*, 79–93. [CrossRef]
72. Puffer, J. Contrasting high field strength element contents of continental flood basalts from plume versus reactivated-arc sources. *Geology* **2001**, *29*, 675–678. [CrossRef]
73. Richards, M.A.; Duncan, R.A.; Courtillot, V.E. Flood Basalts and Hot-Spot Tracks: Plume Heads and Tails. *Science* **1989**, *246*, 103–107. [CrossRef]
74. DePaolo, D.J.; Daley, E. Neodymium isotopes in basalts of the southwest basin and range and lithospheric thinning during continental extension. *Chem. Geol.* **2000**, *169*, 157–185. [CrossRef]
75. Ellam, R. Lithospheric thickness as a control on basalt geochemistry. *Geology* **1992**, *20*, 153–156. [CrossRef]
76. Wang, R.-Q.; Qiu, J.-S.; Yu, S.-B.; Lin, L.; Xu, H. Magma mixing origin for the Quxu intrusive complex in southern Tibet: Insights into the early Eocene magmatism and geodynamics of the southern Lhasa subterrane. *Lithos* **2019**, *328*, 14–32. [CrossRef]
77. Wang, Y.; He, Y.; Wu, H.; Zhu, C.; Huang, S.; Huang, J. Calcium isotope fractionation during crustal melting and magma differentiation: Granitoid and mineral-pair perspectives. *Geochim. Et Cosmochim. Acta* **2019**, *259*, 37–52. [CrossRef]
78. Niu, Y.; Batiza, R. In Situ Densities of Morb Melts and Residual Mantle: Implications for Buoyancy Forces beneath Mid-Ocean Ridges. *J. Geol.* **1991**, *99*, 767–775. [CrossRef]
79. Langmuir, C.H.; Klein, E.M.; Plank, T. Petrological Systematics of Mid-Ocean Ridge Basalts: Constraints on Melt Generation Beneath Ocean Ridges. In *Mantle Flow and Melt Generation at Mid-Ocean Ridges*; American Geophysical Union: Washington, DC, USA, 1992; pp. 183–280. [CrossRef]
80. Johnson, K.T.M.; Dick, H.J.B.; Shimizu, N. Melting in the oceanic upper mantle: An ion microprobe study of diopsides in abyssal peridotites. *J. Geophys. Res. Earth Surf.* **1990**, *95*, 2661–2678. [CrossRef]
81. Grajales-Nishimura, J.; Centeno-Garcia, E.; Keppie, J.; Dostal, J. Geochemistry of paleozoic basalts from the Juchatengo complex of southern Mexico: Tectonic implications. *J. South Am. Earth Sci.* **1999**, *12*, 537–544. [CrossRef]
82. Long, X.; Yigang, X.; Jifeng, X.; Bin, H.; Franco, P. Chemostratigraphy of Flood Basalts in the Garzê-Litang Region and Zongza Block: Implications for Western Extension of the Emeishan Large Igneous Province, SW China. *Acta Geol. Sin. Engl. Ed.* **2004**, *78*, 61–67. [CrossRef]
83. Fu, J.-N.; Pirajno, F.; Yang, F.; Shivute, E.; Sun, Y.-Z.; Ai, N.; Qiu, K.-F. Integration of zircon and apatite U–Pb geochronology and geochemical mapping of the Wude basalts (Emeishan large igneous province): A tool for a better understanding of the tectonothermal and geodynamic evolution of the Emeishan LIP. *Geosci. Front.* **2021**, *12*, 573–585. [CrossRef]
84. Guo, F.; Fan, W.; Wang, Y.; Li, C. When Did the Emeishan Mantle Plume Activity Start? Geochronological and Geochemical Evidence from Ultramafic-Mafic Dikes in Southwestern China. *Int. Geol. Rev.* **2004**, *46*, 226–234. [CrossRef]
85. Shellnutt, J.G.; Pham, T.T.; Denyszyn, S.; Yeh, M.-W.; Tran, T.-A. Magmatic duration of the Emeishan large igneous province: Insight from northern Vietnam. *Geology* **2020**, *48*, 457–461. [CrossRef]

86. Burgess, S.D.; Bowring, S.A. High-precision geochronology confirms voluminous magmatism before, during, and after Earth's most severe extinction. *Sci. Adv.* **2015**, *1*, e1500470. [CrossRef] [PubMed]
87. Schoene, B.; Eddy, M.P.; Samperton, K.M.; Keller, C.B.; Keller, G.; Adatte, T.; Khadri, S.F.R. U-Pb constraints on pulsed eruption of the Deccan Traps across the end-Cretaceous mass extinction. *Science* **2019**, *363*, 862–866. [CrossRef] [PubMed]
88. Schoene, B.; Samperton, K.M.; Eddy, M.P.; Keller, G.; Adatte, T.; Bowring, S.A.; Khadri, S.F.R.; Gertsch, B. U-Pb geochronology of the Deccan Traps and relation to the end-Cretaceous mass extinction. *Science* **2015**, *347*, 182–184. [CrossRef] [PubMed]
89. Zhong, S.; Li, S.; Feng, C.; Gao, Y.; Qu, H.; Seltmann, R.; He, S.; Liu, G.; Wang, X.; Dolgopolova, A. Geochronology and geochemistry of mineralized and barren intrusive rocks in the Yemaquan polymetallic skarn deposit, northern Qinghai-Tibet Plateau: A zircon perspective. *Ore Geol. Rev.* **2021**, *139*, 104560. [CrossRef]
90. Zi, J.W.; Fan, W.; Wang, Y.; Sun, L.H. Geochemical and Sr-Nd isotopic study on Permian basalts from Danba Area, Songpan-Garze Terrane: Petrogenesis and tectonic implication. *Geotecton. Et Metallog.* **2008**, *32*, 226–237.
91. Zhong, H.; Campbell, I.H.; Zhu, W.-G.; Allen, C.M.; Hu, R.-Z.; Xie, L.-W.; He, D.-F. Timing and source constraints on the relationship between mafic and felsic intrusions in the Emeishan large igneous province. *Geochim. Cosmochim. Acta* **2011**, *75*, 1374–1395. [CrossRef]
92. Zhong, H.; Zhu, W.-G.; Chu, Z.-Y.; He, D.-F.; Song, X.-Y. SHRIMP U–Pb zircon geochronology, geochemistry, and Nd–Sr isotopic study of contrasting granites in the Emeishan large igneous province, SW China. *Chem. Geol.* **2007**, *236*, 112–133. [CrossRef]
93. Weiming, F.; Yuejun, W.; Touping, P.; Laicheng, M.; Feng, G. Ar-Ar and U-Pb chronology of Late Paleozoic basalts in Western Guangxi and its constraints on the eruption age of Emeishan basalt province. *Chin. Sci. Bull.* **2004**, *49*, 1892–1900.
94. Boven, A.; Pasteels, P.; Punzalan, L.E.; Liu, J.; Luo, X.; Zhang, W.; Guo, Z.; Hertogen, J. 40Ar/39Ar geochronological constraints on the age and evolution of the Permo-Triassic Emeishan Volcanic Province, Southwest China. *J. Asian Earth Sci.* **2002**, *20*, 157–175. [CrossRef]
95. Lo, C.-H.; Chung, S.-L.; Lee, T.-Y.; Wu, G. Age of the Emeishan flood magmatism and relations to Permian–Triassic boundary events. *Earth Planet. Sci. Lett.* **2002**, *198*, 449–458. [CrossRef]
96. Ali, J.R.; Lo, C.-H.; Thompson, G.M.; Song, X. Emeishan Basalt Ar–Ar overprint ages define several tectonic events that affected the western Yangtze platform in the Mesozoic and Cenozoic ☆. *J. Southeast Asian Earth Sci.* **2004**, *23*, 163–178. [CrossRef]
97. Ali, J.R.; Thompson, G.M.; Zhou, M.-F.; Song, X. Emeishan large igneous province, SW China. *Lithos* **2005**, *79*, 475–489. [CrossRef]
98. He, B.; Xu, Y.-G.; Huang, X.-L.; Luo, Z.-Y.; Shi, Y.-R.; Yang, Q.-J.; Yu, S.-Y. Age and duration of the Emeishan flood volcanism, SW China: Geochemistry and SHRIMP zircon U–Pb dating of silicic ignimbrites, post-volcanic Xuanwei Formation and clay tuff at the Chaotian section. *Earth Planet. Sci. Lett.* **2007**, *255*, 306–323. [CrossRef]
99. Shellnutt, J.G.; Zhou, M.-F.; Yan, D.-P.; Wang, Y. Longevity of the Permian Emeishan mantle plume (SW China): 1 Ma, 8 Ma or 18 Ma? *Geol. Mag.* **2008**, *145*, 373–388. [CrossRef]
100. Zhu, J.; Zhang, Z.C.; Hou, T.; Kang, J.L. LA-ICP-MS zircon U-Pb geochronology of the tuffs on the uppermost of the Emeishan basalt succession in Panxian County, Guizhou Province: Constraints on genetic link between Emeishan large igneous province and the mass extinction. *Acta Petrol. Sin.* **2011**, *27*, 2743–2751.
101. Wang, J.; Shao, L.Y.; Wang, H.; Spiro, B.; Large, D. SHRIMP zircon U–Pb ages from coal beds across the Permian–Triassic boundary, eastern Yunnan, southwestern China. *J. Palaeogeogr.* **2018**, *7*, 117–129. [CrossRef]
102. Kamo, S.; Czamanske, G.; Krogh, T. A minimum U-Pb age for Siberian flood-basalt volcanism. *Geochim. Cosmochim. Acta* **1996**, *60*, 3505–3511. [CrossRef]
103. Renne, P.R.; Basu, A.R. Rapid Eruption of the Siberian Traps Flood Basalts at the Permo-Triassic Boundary. *Science* **1991**, *253*, 176–179. [CrossRef]
104. Claoué-Long, J.; Zichao, Z.; Guogan, M.; Shaohua, D. The age of the Permian-Triassic boundary. *Earth Planet. Sci. Lett.* **1991**, *105*, 182–190. [CrossRef]
105. Ernst, R.; Wingate, M.; Buchan, K.; Li, Z. Global record of 1600–700Ma Large Igneous Provinces (LIPs): Implications for the reconstruction of the proposed Nuna (Columbia) and Rodinia supercontinents. *Precambrian Res.* **2008**, *160*, 159–178. [CrossRef]
106. Hill, R.I. Starting plumes and continental break-up. *Earth Planet. Sci. Lett.* **1991**, *104*, 398–416. [CrossRef]
107. Li, Z.; Bogdanova, S.; Collins, A.; Davidson, A.; De Waele, B.; Ernst, R.; Fitzsimons, I.; Fuck, R.; Gladkochub, D.; Jacobs, J.; et al. Assembly, configuration, and break-up history of Rodinia: A synthesis. *Precambrian Res.* **2008**, *160*, 179–210. [CrossRef]
108. Li, Z.; Li, X.; Kinny, P.; Wang, J. The breakup of Rodinia: Did it start with a mantle plume beneath South China? *Earth Planet. Sci. Lett.* **1999**, *173*, 171–181. [CrossRef]
109. Saunders, A.D.; England, R.W.; Reichow, M.K.; White, R.V. A mantle plume origin for the Siberian traps: Uplift and extension in the West Siberian Basin, Russia. *Lithos* **2005**, *79*, 407–424. [CrossRef]
110. Saunders, A.D.; Storey, M.; Kent, R.W.; Norry, M.J. Consequences of Plume-Lithosphere Interactions. In *Magmatism and the Causes of Continental Break-Up*; Storey, B.C., Alabaster, T., Pankhurst, R.J., Eds.; Geological Society: London, UK, 1992; Volume 68, pp. 41–60. [CrossRef]
111. Weislogel, A.L. Tectonostratigraphic and geochronologic constraints on evolution of the northeast Paleotethys from the Songpan-Ganzi complex, central China. *Tectonophysics* **2008**, *451*, 331–345. [CrossRef]
112. Yin, A.; Harrison, T.M. Geologic evolution of the Himalayan-Tibetan orogen. *Annu. Rev. Earth Planet. Sci.* **2000**, *28*, 211–280. [CrossRef]

113. Chen, X.; Rong, J.Y.; Rowley, D.E.; Zhang, J.; Zhang, Y.D.; Zhan, R.B. A Query on the Early Paleozoic Banxi Ocean in South China. *Geol. Rev.* **1995**, *41*, 389–400.
114. Luo, Z.L. A discussion of taphrogenesis and hydrocarbon distribution in China. *Acta Geosci. Sin.* **1984**, *10*, 93–101.
115. Luo, Z.L. The dynamical model of the lithospheric evolution in longmenshan orogenic belt. *J. Chengdu Univ. Technol.* **1991**, *18*, 1–7.
116. Luo, Z.L. The rise of Longmenshan orogenic belt and the formation and evolution of Sichuan Basin. *J. Chengdu Univ. Technol.* **1994**, *1*, 564.
117. Luo, Z.L.; Long, X.M. The uplifting of the Longmenshan orogenic zone and the subsidence of the west Sichuan foreland basin. *Acta Geol. Sichuan* **1992**, *12*, 1–17.
118. Li, L.; Jin, G.Y. Telluric electromagnetic sounding study of crust and upper mantle in the Panxi "rift zone" and the Longmenshan faulted zone. *Geophys. Geochem. Explor.* **1987**, *11*, 161–169.
119. Xue, Z. *Mesozoic Tectonic Evolution of the Longmenshan Thrust Belt*; University of China Academy of Sciences: Beijing, China, 2017.
120. Condie, K.C. *Mantle Plumes and their Record in Earth History*; Cambridge University Press: Cambridge, UK, 2001. [CrossRef]
121. McKenzie, D.; O'Nions, R.K. The Source Regions of Ocean Island Basalts. *J. Pet.* **1995**, *36*, 133–159. [CrossRef]
122. Morgan, W.J. Deep Mantle Convection Plumes and Plate Motions. *AAPG Bull.* **1972**, *56*, 203–213. [CrossRef]
123. He, B.; Xu, Y.; Wang, Y.; Luo, Z. Sedimentation and Lithofacies Paleogeography in Southwestern China Before and After the Emeishan Flood Volcanism: New Insights into Surface Response to Mantle Plume Activity. *J. Geol.* **2006**, *114*, 117–132. [CrossRef]
124. Song, X.Y.; Hou, Z.Q.; Wang, Y.L.; Zhang, C.J.; Cao, Z.M. The mantel plume features of Emeishan basalts. *J. Mineral. Petrol.* **2002**, *4*, 27–32.
125. Zhang, Z.; Kang, J.; Kusky, T.; Santosh, M.; Huang, H.; Zhang, D.; Zhu, J. Geochronology, geochemistry and petrogenesis of Neoproterozoic basalts from Sugetbrak, northwest Tarim block, China: Implications for the onset of Rodinia supercontinent breakup. *Precambrian Res.* **2012**, *220–221*, 158–176. [CrossRef]
126. He, B.; Xu, Y.-G.; Chung, S.-L.; Xiao, L.; Wang, Y. Sedimentary evidence for a rapid, kilometer-scale crustal doming prior to the eruption of the Emeishan flood basalts. *Earth Planet. Sci. Lett.* **2003**, *213*, 391–405. [CrossRef]
127. Xu, Y.-G.; He, B.; Huang, X.-L.; Luo, Z.; Chung, S.-L.; Xiao, L.; Zhu, D.; Shao, H.; Fan, W.-M.; Xu, J.; et al. Identification of mantle plumes in the Emeishan Large Igneous Province. *Epis. J. Int. Geosci.* **2007**, *30*, 32–42. [CrossRef]
128. Zhao, L.; Graham, I. Origin of the alkali tonsteins from southwest China: Implications for alkaline magmatism associated with the waning stages of the Emeishan Large Igneous Province. *Aust. J. Earth Sci.* **2016**, *63*, 123–128. [CrossRef]
129. Chen, D.; Zhou, X.; Fu, Y.; Wang, J.; Yan, D. New U-Pb zircon ages of the Ediacaran-Cambrian boundary strata in South China. *Terra Nova* **2014**, *27*, 62–68. [CrossRef]
130. Chen, Y.; Xu, Y.; Xu, T.; Si, S.; Liang, X.; Tian, X.; Deng, Y.; Chen, L.; Wang, P.; Xu, Y.; et al. Magmatic underplating and crustal growth in the Emeishan Large Igneous Province, SW China, revealed by a passive seismic experiment. *Earth Planet. Sci. Lett.* **2015**, *432*, 103–114. [CrossRef]
131. Zhang, Z.M.; Liou, J.; Coleman, R. An outline of the plate tectonics of China. *Geol. Soc. Am. Bull.* **1984**, *95*, 295–312. [CrossRef]